

CORRELATION PROPERTIES OF THE KINEMATIC SUNYAEV-ZEL'DOVICH EFFECT AND IMPLICATIONS FOR DARK ENERGY

CARLOS HERNÁNDEZ-MONTEAGUDO,¹ LICIA VERDE,¹ RAUL JIMENEZ¹ AND DAVID N. SPERGEL²

Draft version August 30, 2018

ABSTRACT

In the context of a cosmological study of the bulk flows in the Universe, we present a detailed study of the statistical properties of the kinematic Sunyaev-Zel'dovich (kSZ) effect. We first compute analytically the correlation function and the power spectrum of the projected peculiar velocities of galaxy clusters. By taking into account the spatial clustering properties of these sources, we perform a line-of-sight computation of the *all-sky* kSZ power spectrum and find that at large angular scales ($l < 10$), the local bulk flow should leave a visible signature above the Poisson-like fluctuations dominant at smaller scales, while the coupling of density and velocity fluctuations should give much smaller contribution. We conduct an analysis of the prospects of future high resolution CMB experiments (such as ACT and SPT) to detect the kSZ signal and to extract cosmological information and dark energy constraints from it. We present two complementary methods, one suitable for “deep and narrow” surveys such as ACT and one suitable for “wide and shallow” surveys such as SPT. Both methods can constraint the equation of state of dark energy w to about 5-10% when applied to forthcoming and future surveys, and probe w in complementary redshift ranges, which could shed some light on its time evolution. This is mainly due to the high sensitivity of the peculiar velocity field to the onset of the late acceleration of the Universe. We stress that this determination of w does not rely on the knowledge of cluster masses, although it relies on cluster redshifts and makes minimal assumptions on cluster physics.

Subject headings: cosmic microwave background – large scale structure of universe

1. INTRODUCTION

The new generation of ground-based high-resolution cosmic microwave background (CMB) experiments (e.g., the Atacama Cosmology Telescope³ [ACT;Kosowsky (2003); Fowler et al. (2005)] and the South Pole Telescope⁴ [SPT;Ruhl et al. (2004)]), are designed to scan with very high sensitivity and arcminute resolution the microwave sky. Their main goal is the study of the thermal Sunyaev-Zel'dovich (tSZ) effect (Sunyaev & Zel'dovich 1980): the change of frequency of CMB photons due to inverse Compton scattering by hot electrons. Such hot electron plasma are known to be found in clusters of galaxies, and should also be present in larger structures, such as filaments and superclusters of galaxies. This scattering translates into a redshift independent distortion of the CMB black body spectrum, making the tSZ effect an ideal tool to probe the baryon distribution in the large scales of our Universe at different cosmic epochs. However, this is not the only effect of an electron plasma on the CMB radiation. If a cloud of electrons is moving with some bulk velocity with respect to the CMB frame, then Thomson scattering by these electrons will imprint new (Doppler induced) temperature fluctuations on the CMB photons. This is the so called kinematic Sunyaev-Zel'dovich effect (kSZ, Sunyaev & Zeldovich (1972)), which is spectrally indistinguishable from the intrinsic CMB temperature fluctuations.

Although the kSZ effect is typically an order of magnitude smaller than the tSZ in clusters of galaxies (and for this reason much harder to detect), it encodes precious cosmological

information since it depends on the peculiar velocity field. Indeed, kSZ measurements can yield valuable information about the large-scale velocity field, the evolution of the dark matter potential, and the growth of fluctuations. The study of large scale velocity fields (cosmic flows) has been an active research area in the nineties. There have been numerous attempts to measure bulk flows using the large-scale distribution of galaxies and their peculiar velocities, and to place constraints on the matter power spectrum or the Universe matter density, (see reviews of Strauss & Willick (1995) and Courteau & Dekel (2001) and references therein). However, it became clear that these measurements had to be corrected for systematic errors, such as the biases introduced when calibrating the distances of the galaxies under study, or the non linear components of the velocities of those objects. With kSZ observations, by using clusters as tracers of the velocity fields, one is more confident to probe larger (less non-linear) scales.

While there have been no kSZ detections to date, upper limits on the peculiar velocities of individual clusters have been reported by Benson et al. (2003). Such a difficult measurement could in principle be hampered by other effects such as non-linearities and the complicated physics of the intra-cluster gas. Nagai, Kravtsov, & Kosowsky (2003) have shown that the kSZ is not diluted by the internal velocity dispersion in the intracluster gas. Ma & Fry (2002) calculated the temperature fluctuations produced by the kSZ in the non-linear regime using the halo model. Benson et al. (2003) showed that the signal-to-noise of a kSZ measurement should be distance independent and suggested combining signals from different redshifts. Holder (2002) and Aghanim et al. (2004) have discussed how to extract the kSZ signal from maps, while Schäfer et al. (2004) used N-body simulations to build templates of kSZ maps in the context of the Planck mission, and Kashlinsky & Atrio-Barandela (2000) study the possibility of extracting the kSZ dipole from

¹ Department of Physics and Astronomy, University of Pennsylvania, 209 South 33rd St, Philadelphia, PA 19104; carloshm@astro.upenn.edu, lverde,raulj@physics.upenn.edu

² Department of Astrophysical Sciences, Peyton Hall, Princeton University, Princeton, NJ 08540; dns@astro.princeton.edu

³ <http://www.hep.upenn.edu/act/>

⁴ <http://spt.uchicago.edu/>

CMB surveys covering a large fraction of the sky. Due to its weak signal, indirect detection of the kSZ has been proposed through cross-correlation techniques with weak-lensing (Doré, Hennawi, & Spergel 2004) or old galaxies (DeDeo, Spergel & Trac 2005). As we shall see below, a measurement of the kSZ effect would be very valuable, since it would not only allow us to measure bulk flows of clusters of galaxies and test the predictions of the standard model, but also provide additional constraints on cosmological parameters, especially on the equation of state of dark energy.

In this paper we compute the correlation function and the power spectrum of the kSZ effect. This requires modeling of the peculiar velocity field and the cluster population. We explore the prospects for future CMB experiments to measure the kSZ correlation function, and find that ACT-like experiments should be able to detect the kSZ-induced CMB variance at high ($\sim 12\sigma$) significance level. Further, we study the dependence of the kSZ correlation function on the cosmological parameters, and show that it can be used to measure the equation of state of dark energy (w) if the redshifts of the clusters of galaxies detected in CMB surveys are available. We find that, with the SALT follow up of ACT data or with a wider but shallower (SPT-like) survey, the w parameter can be constrained with an accuracy of 8% for an ACT scan of 400 square degrees. This error should scale inversely with the square root of the covered area and hence becomes 5% for a 1,000 square degree area. These determinations of w do not rely on the knowledge of cluster masses, but do rely on clusters redshifts and reasonable assumptions on cluster physics.

Unless otherwise stated, throughout this work we shall assume a Λ CDM cosmological model (Spergel et al. 2003) with $\Omega_m = 0.3$, $\Omega_\Lambda = 0.7$, $h = 0.72$, and $\sigma_8 = 0.88$. The paper is organised as follows: in Section 2 we study the statistical properties of the projected peculiar velocity field and provide an analytical expression for the correlation function of projected velocities. In Section 3 we compare the kSZ and tSZ effects, and discuss the strategy to enhance the probabilities of detecting the former. In Section 4 we compute the correlation function and the power spectrum of the kSZ, both when we consider only a given set of clusters present in a survey or the whole celestial sphere. In Section 5 we outline two methods to estimate the kSZ effect in future CMB cluster surveys and in Section 6 we explore the dependence of kSZ measurements on cosmological parameters making particular emphasis on w . We conclude in Section 7.

2. THE CORRELATION FUNCTION OF LINE-OF-SIGHT LINEAR PECULIAR VELOCITIES

While the measurement of the kSZ effect of individual clusters is difficult (e.g., Aghanim et al. (2001); Benson et al. (2003)), in this paper we address the prospects for statistical detection of cluster peculiar velocities in future CMB surveys. This requires the knowledge of the ensemble properties of the velocity field traced by the galaxy cluster population, to which we devote the current section. For clarity and future reference, a statistical description of the linear velocity field and related quantities is given in Appendix A.

Throughout this paper, we shall assume that the measured velocity field obeys linear theory. However, as noted by Colberg et al. (2000), this is not completely fulfilled by cluster velocities, since clusters are peculiar tracers of the large scale matter distribution and show *biased* velocities

compared to the expectations provided by the linear theory. Colberg et al. (2000) found that this bias was typically a 30% - 40% effect. Although several attempts have been made to model this boost in terms of the underlying density field (Sheth & Diaferio 2001; Hamana et al. 2003), in subsequent sections it will be accounted for by simply increasing the cluster velocities by a factor $b_v = 1.3$ (Sheth & Diaferio 2001). The goal of this paper is to present a theoretical calculation of the detectability of the signal and the forecasted signal-to-noise: detailed comparison with numerical simulations are left to future work. Full treatment can be implemented only with the help of numerical simulations matched to a given observing program (see Peel (2005) for a recent study). We must stress that, although some modelling of non-linear effects must be included in this study, clusters are the largest virialised structures known in the Universe, and probe much bigger scales than galaxies. Therefore we must expect them to be significantly better tracers of the linear velocity field. Furthermore, as we shall see below, the peculiar velocity estimator (the kSZ effect) does *not* depend of distance, which avoids the need to use redshift-independent distance indicators, as opposed to other peculiar velocity estimators.

On large, linear scales, the density and peculiar velocities are related through the continuity equation: $\partial\delta_{\mathbf{k}}/\partial t = -i\mathbf{k} \cdot \mathbf{v}_{\mathbf{k}}/a$, where a and k are the scale factor and comoving Fourier mode, respectively. The peculiar velocity of a cluster, as probed by its kSZ effect, can be interpreted as the linear peculiar velocity field smoothed on comoving scale R which corresponds to the cluster's mass M via

$$R = \left[\frac{3M}{4\pi\bar{\rho}} \right]^{1/3}, \quad (1)$$

where $\bar{\rho}$ is the background matter density. The kSZ effect is sensitive to the line-of-sight component of the velocity, but under the assumption that the velocity field is Gaussian and isotropic (which should be satisfied in the linear regime) the three spatial components of the velocity field must be statistically independent. Moreover, the power spectrum must completely determine the statistical properties of the velocity field. Thus, in a given cosmological model, the linear velocity field power spectrum (which in turn is related to the matter power spectrum) should univocally determine the angular correlation function (and angular power spectrum) of the line-of-sight cluster velocities.

In linear theory, the velocity dispersion smoothed over spheres of comoving radius R (corresponding to a given cluster mass M) is given by

$$\sigma_{vv}^2(R, z) = \left(H(z) \left| \frac{d\mathcal{D}_\delta}{dz} \right| \right)^2 \int dk k^2 \frac{P_m(k)}{2\pi^2 k^2} |W(kR)|^2, \quad (2)$$

where $W(kR)$ is the Fourier transform of the top hat window function, $H(z)$ is the Hubble function, $\mathcal{D}_\delta(z)$ is the linear growth factor and $P_m(k)$ is the present day linear matter power spectrum, (the power spectra at any redshift will be denoted as $P_{\delta\delta}(z, k) \equiv \mathcal{D}_\delta^2(z) P_m(k)$). Hence the power spectrum of the velocities is:

$$P_{vv}(k) = \left(H(z) \left| \frac{d\mathcal{D}_\delta}{dz} \right| \right)^2 \frac{P_m(k)}{k^2} = \mathcal{D}_v^2 \frac{P_m(k)}{k^2}, \quad (3)$$

where $\mathcal{D}_v \equiv H(z) d\mathcal{D}_\delta/dz$ is the velocity growth factor. When computing \mathcal{D}_δ for different Dark Energy models, we used the

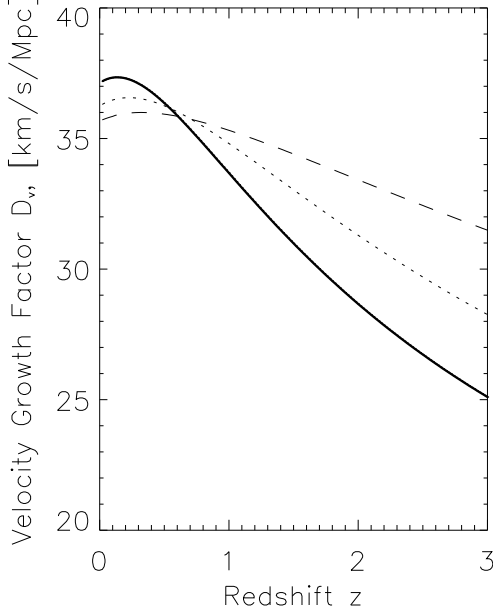


FIG. 1.— Peculiar velocity growth factor for three different cosmologies: a Λ CDM model ($\Omega_L = 0.7$, $\Omega_m = 0.3$, thick solid line), a $\Omega_m = 0.3$, flat $w = -0.6$ model (dotted line), and $\Omega_m = -1/3$ and $w = -1/3$, (dashed line).

analytical fit provided by Linder (2005):

$$g(a) = \exp \int_0^a d \log a \left[\left(\Omega_m \frac{H_0^2}{a^3 H^2(a)} \right)^\gamma - 1 \right], \quad (4)$$

where $g(a) \equiv \mathcal{D}_\delta(a)/a$ gives the deviation of the growth factor from that of a critical ($\Omega_m = 1$) universe, and γ is given by

$$\gamma = 0.55 + b[1 + w(z=1)], \quad (5)$$

with $b = 0.05$ if $w > -1$ and $b = 0.02$ otherwise.

The growth of the velocity perturbations with redshift may provide useful cosmological constraints such as constraints on the equation of state of dark energy (DeDeo, Spergel & Trac 2005). This is illustrated in Fig.(1), where we show the redshift evolution of the velocity growth factor for three different cosmological models: a Λ CDM model ($\Omega_\Lambda = 0.7$, $\Omega_m = 0.3$, thick solid line), a flat universe with $\Omega_m = 0.3$ and dark energy equation of state parameter $w = -0.6$ (dotted line), and another flat model with $\Omega_m = 0.3$ and $w = -1/3$, (dashed line). Due to the k^2 factor in the denominator of eq.(3), the signal is weighted by the largest scales, making this probe relatively insensitive to the smoothing scale and therefore to clusters mass. Indeed, if the dependence of σ_{vv} versus mass is approximated by a power law, then one finds that for the concordance model $\sigma_{vv} \propto M^{-0.13}$.

Having this in mind, we compute here the angular correlation function of the *line-of-sight* (LOS) cluster velocities. Note that Peel (2005) takes a different approach to this calculation. Assuming that we can measure the LOS component of the peculiar velocity of a cluster, we compute the quantity

$$C_{vv}(\theta_{12}) \equiv \langle (\mathbf{v}(\mathbf{x}_1) \cdot \mathbf{n}_1) (\mathbf{v}(\mathbf{x}_2) \cdot \mathbf{n}_2) \rangle, \quad (6)$$

where \mathbf{n}_1 and \mathbf{n}_2 denote two different directions in the sky, “connecting” the observer to the cluster positions \mathbf{x}_1 and \mathbf{x}_2 and θ_{12} denotes the angle between \mathbf{n}_1 and \mathbf{n}_2 . We refer the reader to Appendix B for the detailed derivation and here we report the final expression for this correlation function:

$$C_{vv}(\theta_{12}) = \sum_{\text{even } l} \frac{2l+1}{4\pi} \cos \theta_{12} \times \left(\frac{2}{\pi} \mathcal{F}_l \right) \int k^2 dk P_{vv}(k) W(kR_1) W(kR_2) \times j_l(k[x_1 - x_2 \cos \theta_{12}]) j_l(kx_2 \sin \theta_{12}), \quad (7)$$

In this equation, the factor \mathcal{F}_l is given by

$$\mathcal{F}_l \equiv \frac{(l-1)!!}{2^{l/2} (l/2)!} \cos l\pi/2, \quad (8)$$

and x_1, x_2 are the (comoving) distances to the clusters, (without loss of generality we have used the convention that $x_1 \geq x_2$). Here $j_l(x)$ denote the spherical Bessel functions and the summation must take place only over *even* values of l ; R_1 and R_2 refer to the linear scales corresponding to the masses of each cluster. Note that we recover eq.(2) in the limit of $\theta_{12} \rightarrow 0$ and $x_1 \rightarrow x_2$.

Fig.(2a) shows the behaviour of C_{vv} vs θ_{12} in the concordance Λ CDM model for a couple of $10^{14} M_\odot$ clusters when they are both placed at $z=0.005$ (solid line), both placed at $z=0.1$ both (dashed line) and when once cluster is at $z=0.1$ and the other at $z=1$ (dotted line). In the first (clearly unrealistic) case, the clusters are so close to us that both are comoving in the same bulk flow with respect to the CMB frame, giving rise to the dipolar pattern shown by the solid line. In the case where both clusters are at $z \sim 0.1$ (dashed line), their correlation properties are strongly dependent on θ_{12} , since this angle defines the distance between the clusters. For small angular separation, the clusters are still relatively nearby, and hence their peculiar velocities are correlated, but this correlation dies as the separation of the clusters increases. The angular distance at which the correlation drops to half its value at zero separation is $\sim 10^\circ$, corresponding to roughly $40 h^{-1}$ Mpc. Finally, if clusters are very far apart from each other (thick dotted line), their peculiar velocities are not correlated.

An alternative way to present the correlation properties of the projected peculiar velocities of the clusters is the velocity field angular power spectrum. In Appendix B, we invert $C_{vv}(\theta_{12})$ into its angular power spectrum C_l^{vv} , i.e.,

$$C_{vv}(\theta_{12}) = \sum_l \frac{2l+1}{4\pi} C_l^{vv} P_l(\cos \theta_{12}). \quad (9)$$

We find that

$$C_l^{vv} \equiv \frac{4\pi}{2l+1} (lB_{l-1} + (l+1)B_{l+1}), \quad (10)$$

where the B_l coefficients are defined by

$$B_l \equiv 4\pi \int \frac{k^2 dk}{(2\pi)^3} P_{vv}(k) j_l(kx_1) j_l(kx_2) \quad (11)$$

Fig.(2b) displays the power spectra for two cases: two very nearby clusters (both at $z=0.005$, solid line), showing an almost dipolar pattern, and two relatively far away clusters

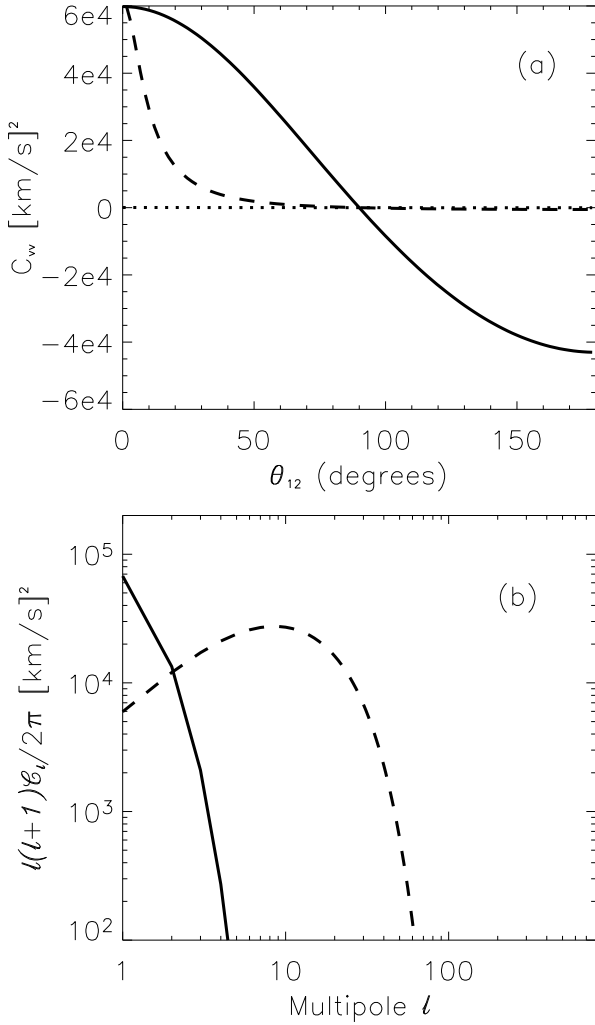


FIG. 2.— Correlation function (top) and corresponding power spectrum (bottom) of the projected peculiar proper velocities. The solid lines observe the case where the two clusters are placed at $z = 0.005$ from the observer. Dashed lines show the case in which clusters are further, $z = 0.01$. Finally, the dotted line considers the case where one cluster is located at $z = 0.1$ and the other cluster is much further ($z = 1$). Note the lack of correlation in this case.

(both at $z=0.1$, dashed line), case in which the power is transferred to higher multipoles. The power spectrum for the clusters placed at $z=0.005$ and $z=0.1$ is zero.

Here we have characterised the projected peculiar velocity field at cluster scales. Next, we address the study of the kSZ effect and its comparison with the tSZ effect.

3. THE SUNYAEV-ZEL'DOVICH EFFECTS

3.1. The kinematic Sunyaev-Zel'dovich Effect

The Kinematic Sunyaev-Zel'dovich effect describes the Doppler kick that CMB photons experience when they encounter a moving cloud of electrons. Since this is simple Thomson scattering, there is no change of the photon frequency, and hence it leaves no spectral signatures in the CMB blackbody spectrum. Therefore, this effect is solely determined by the number density of free electrons and their rel-

ative velocity to the CMB frame. An observer will only be sensitive to the *radial* component of the electron peculiar velocity, so the expression for the change in brightness temperature becomes (Sunyaev & Zel'dovich 1968)

$$\frac{\delta T_{\text{kSZ}}}{T_0} = \int dl n_e(l) \sigma_T \left(-\frac{\mathbf{v} \cdot \mathbf{n}}{c} \right) \equiv \tau \left(-\frac{\mathbf{v} \cdot \mathbf{n}}{c} \right). \quad (12)$$

Here, we have assumed that the peculiar velocity is the same for all electrons. τ stands for the optical depth, and \mathbf{n} is a unitary vector giving the direction of observation. This process must take place in two contexts: (1) When the intergalactic medium becomes ionized by the high energy photons emitted by the first stars, inhomogeneities in the electron velocity and density distributions generate a kSZ signal which is known as the Ostriker-Vishniac effect. Despite of the large size of ionized structures encountered by the CMB photons, the electron density contrast is relatively small, and further, we do not know where in CMB maps to look for this signal because we do not know the location of the ionized bubbles which formed during reionization. The amplitudes and angular scales at which this effect should be visible are model dependent, but can be as high as a few microK in the multipole range $l > 2000$, (Santos et al. 2003). (2) Clusters of galaxies at lower redshift leave a more easily detectable signal. Their high electron density can give rise to values of τ as high as $10^{-3} - 10^{-2}$, and their peculiar velocities should be close to 300 km s^{-1} at $z = 0$, which together can produce temperature fluctuations of the order of $1-10 \mu\text{K}$. The clusters high optical depth is also responsible for large spectral distortions of the CMB generated through the thermal Sunyaev-Zel'dovich (tSZ) effect. The tSZ effect is typically an order of magnitude larger than the kSZ and introduces *frequency dependent* brightness temperature fluctuations which, in the not relativistic limit, change sign at 218 GHz. Therefore by combining observations in bands at frequencies lower and higher than this cross frequency, it is possible to obtain the cluster position and to characterize the tSZ cluster signal. Once the cluster position is identified their kSZ contribution should be accessible at 218 GHz. However, as noted by Sehgal, Kosowsky & Holder (2005) and earlier by Holder (2004), even with measurements in three different frequencies it may not be possible to obtain a clean estimate of the kSZ effect for a single cluster. We shall show below that we are not interested in a very accurate kSZ estimate for a given cluster, but on *unbiased* estimates on our entire cluster sample.

In the next subsection we make a detailed comparison of the amplitude of the kSZ and the tSZ effects.

3.2. Comparison of the kSZ and the tSZ effects in clusters of galaxies

In what follows we shall describe the galaxy cluster population by adopting the model presented in Verde, Haiman & Spergel (2002). This model is based upon the spherical collapse description of galaxy clusters (Gunn & Gott 1972), and assumes that clusters are isothermal and their gas acquires the virial temperature of the halo. The halo mass and redshift distribution is approximated by the formalism presented in Sheth & Tormen (1999). We refer to Verde, Haiman & Spergel (2002) for further details in this modelling.

Both kSZ and tSZ effects can be written as integrals of some function $\mathcal{K}(r)$ along the line of sight crossing the cluster, weighted by the electron density:

$$\frac{\delta T}{T_0} = g(x) \int dl \sigma_T n_e(l) \mathcal{K}(l) \quad (13)$$

For the non-relativistic tSZ $g(x) = (x \coth x/2 - 4)$, $x \equiv h\nu/k_B T_0$ is the adimensional frequency in terms of the CMB monopole T_0 , $\mathcal{K} = k_B T_e/(m_e c^2)$ where n_e , T_e , m_e are the electron density, temperature and mass respectively, σ_T the Thomson cross-section and k_B the Boltzmann constant. For the kSZ, $g(x) \equiv 1$, $\mathcal{K} = -\mathbf{n} \cdot \mathbf{v}/c$, where \mathbf{n} is a unitary vector pointing along the line of sight, and \mathbf{v} is the cluster peculiar velocity. If clusters are perfectly virialised objects, then one must expect the scaling $T_e \propto M^{2/3}$. However, following Verde, Haiman & Spergel (2002), the cluster model should leave some room for some deviations from such scaling, which can be due to internal (non-linear) cluster physics, deviations from purely gravitational equilibrium, preheating, etc. Our parametrization adopts $T_e \propto M^{1/\xi}$, where $\xi = 1.5$ for a perfectly virialized cluster, but spans the range from 1.5 to 2 in the literature. We shall present results for $\xi = 1.5$, but the sensitivity of our results on ξ is minimal. At the same time, the radial peculiar velocity dispersion of the clusters, $\langle \sqrt{(-\mathbf{n} \cdot \mathbf{v}/c)^2} \rangle = \sigma_{vv}$ decreases very slowly with mass ($\sim M^{-0.13}$), so, at fixed redshift we must expect the ratio kSZ/tSZ to be bigger for low mass clusters, which are more numerous. Regarding the redshift dependence, clusters tend to be denser at earlier epochs (the product $n_e r_v$ scales roughly as $(1+z)^2$), so we must expect larger tSZ and kSZ amplitudes at higher redshifts. However, the dependence of the function \mathcal{K} is different in each case: while clusters are hotter at earlier times ($T_e \propto (1+z)$), velocities have not had so much time to grow as at present epochs ($\sigma_{vv} \propto 1/\sqrt{1+z}$), and hence the ratio kSZ/tSZ ($\propto 1/(1+z)^{3/2}$) decreases with redshift.

We show these scalings explicitly in Fig.(3), where the thin lines evaluate the tSZ and the kSZ at $z = 0$ and thick lines correspond to $z = 1$. The solid lines provide the amplitude of the cluster-induced tSZ fluctuations at 222 GHz, which, as we shall see below, will be taken as our effective frequency after accounting for the tSZ relativistic corrections and the effects related to the finite spectral width of the detectors. The dashed lines provide the expected rms amplitude of the kSZ effect in clusters: we see that, at $z = 0$, clusters of masses below $\sim 10^{15} M_\odot$ should produce more kSZ than tSZ flux at 222 GHz, at least by a factor of a few. This mass threshold decreases at $z = 1$, but so does the typical halo mass at such redshift (clusters of $\sim 10^{14} M_\odot$ are very rare objects), so again we must expect the kSZ to dominate over the tSZ.

4. THE POWER SPECTRUM OF THE KSZ EFFECT

4.1. Model of the cluster population

We next study the kSZ signal generated by the entire population of clusters of galaxies by computing its two second-order momenta, i.e., the correlation function and the power spectrum. For this, it is first necessary to have a model to describe the population of galaxy clusters in the Universe. We shall adopt the hierarchical scenario in which small scale overdensities in the Universe become non-linear and collapse first, and then merge and give rise to bigger non-linear structures. The abundance of haloes of a given mass at a given

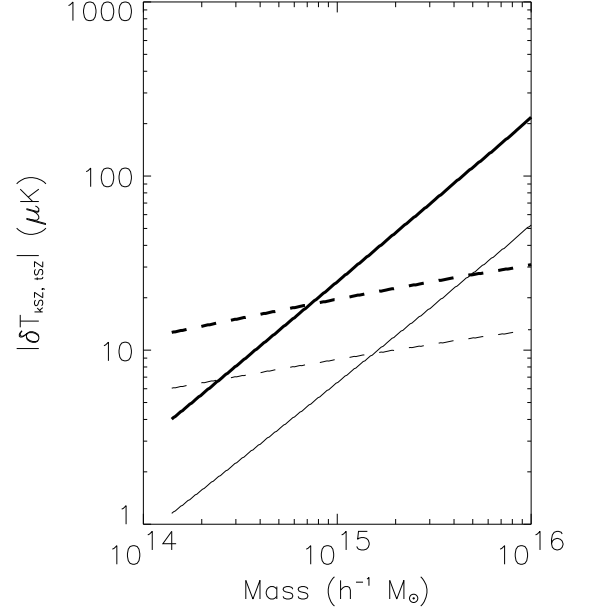


FIG. 3.— Comparison of the tSZ (solid lines) and kSZ (dashed line) effects as a function of clusters mass. Thick lines refer to $z=1$ (where most of the clusters are located for ACT-like surveys), whereas thin lines correspond to $z=0$. For the majority of clusters, the kSZ flux will be a few times bigger than the tSZ flux at 222 GHz.

cosmic epoch or redshift is given by the clusters mass function. We will adopt the Sheth & Tormen (hereafter ST) mass function (Sheth & Tormen 1999), which will be denoted by $\bar{n}(M, z) \equiv dN(M, z)/dV(z)$ and provides the *average* number density of haloes of mass contained between M and $M+dM$ at redshift z . It must not be confused with $n(M, \mathbf{x})$, which is the *actual* number of haloes in that mass range at position \mathbf{x} . The latter can be understood as a *random* variable, the former as its *mean*. As it will be useful later, we first compute the mean number of haloes present in two volume elements centered at \mathbf{x}_1 and \mathbf{x}_2 :

$$\begin{aligned} \langle n(M_1, \mathbf{x}_1) n(M_2, \mathbf{x}_2) \rangle &= \bar{n}(M_1, z_1) \bar{n}(M_2, z_2) + \\ &\delta_D(M_1 - M_2) \delta_D^3(\mathbf{x}_1 - \mathbf{x}_2) \bar{n}(M_1, z_1) + \\ &\langle \Delta[n(M_1, \mathbf{x}_1)] \Delta[n(M_2, \mathbf{x}_2)] \rangle. \end{aligned} \quad (14)$$

In this equation, z_1 and z_2 are the redshift corresponding to positions \mathbf{x}_1 and \mathbf{x}_2 respectively. The first term in the right hand side of the equation is merely a constant, but will have its relevance, because it will couple with the velocity field as we shall see below. The next term containing the Dirac deltas accounts for the (assumed) Poissonian statistics ruling the (discrete) number density of sources, and will be referred to as the *Poissonian* term. In the third term, $\Delta[n(M_1, \mathbf{x}_1)]$ stands for the deviation with respect to the average halo number density due to the environment, i.e., due to large scale overdensities, which condition the halo clustering. Therefore, this third term describes the spatial clustering of haloes, which is a biased tracer of the spatial clustering of matter. In the extended Press-Schechter approach it can be shown that the power spectrum and the correlation function of haloes and underlying matter are merely proportional to each other over a

wide range of scales. This is commonly expressed by a *bias factor* (Mo & White 1996), so that

$$\xi_{hh}(r) = b^2(M, z) \xi_m(r); \quad P_{hh}(k) = b^2(M, z) P_m(k). \quad (15)$$

Here ξ_{hh}, ξ_m and $P_{hh}(k), P_m(k)$ stand for halo-halo and matter correlation function/power spectrum, respectively. Therefore, the third term in the RHS of eq.(14) equals $\bar{n}(M_1, z_1) \bar{n}(M_2, z_2) b(M_1, z_1) b(M_2, z_2) \xi_m(\mathbf{x}_1 - \mathbf{x}_2)$.

A parallel approach consists in writing the halo mass function as a function of some linear scale matter overdensity $\delta \equiv (\rho - \bar{\rho}) / \bar{\rho}$. The number of haloes at \mathbf{x} is then approximated as

$$n(M, \mathbf{x}) = \bar{n}(M, z) + \eta + \left. \frac{\partial \bar{n}(M, z)}{\partial \delta} \right|_{\delta=0} \delta(\mathbf{x}) + \mathcal{O}[\delta^2], \quad (16)$$

where η is a random variable which introduces the Poissonian behaviour of the source counts. In the extended Press-Schechter formalism, it turns out that $\partial \bar{n}(M, z) / \partial \delta|_{\delta=0}$ coincides with the bias factor $b(M, z)$, and by using this it is possible to reproduce eq. (14) from eq.(16). This justifies neglecting all higher-order powers of δ in eq. (16). We have taken δ to be in *linear* regime, but, since $\xi_{hh}(r) \simeq b^2 \xi_{mm}(r)$ down to scales comparable to the halo size, we shall use this formalism down to halo scales.

4.2. A Line of Sight approach for the kSZ effect

We next write the temperature anisotropies induced by the kSZ in clusters of galaxies as an integral along the line of sight:

$$\frac{\Delta T_{kSZ}}{T_0}[\mathbf{n}] = \int_0^{r_{lss}} dr \sum_j \dot{\tau}_j \left(-\frac{\mathbf{v}_j \cdot \mathbf{n}}{c} \right) W_j^{gas}(\mathbf{r} - \mathbf{r}_j). \quad (17)$$

Here, r is the comoving radius integrated to the last scattering surface, and the sum over the index j represents a sum on all clusters; $\dot{\tau}_j$ denotes the opacity in the *center* of the cluster ($\dot{\tau} = a \sigma_T n_{e,c}$ with $n_{e,c}$ the central electron number density and a the scale factor), and the window function $W_j^{gas}(\mathbf{r} - \mathbf{r}_j)$ denotes the gas profile of the cluster. Although we should adopt some realistic shape for this profile (Komatsu & Seljak 2001), we have adopted a simple Gaussian window with scale radius equal to the virial radius of the cluster. This is justified since, in Fourier domain, at scales bigger than the cluster size, the window function is merely equal to the volume occupied by the gas, regardless of the shape of the gas profile. This step simplifies our computations significantly, *and* does not compromise the accuracy in the relatively big scales (bulk flow scales) in which we are interested. Note that even if the sum is made over all clusters, *only* the clusters being intersected by the line of sight will contribute to the integral. This sum can be re-written first as an integral and then as a convolution,

$$\begin{aligned} \frac{\Delta T_{kSZ}}{T_0}[\mathbf{n}] &= \int_0^{r_{lss}} dr \int dM \times \\ &\left(\int d\mathbf{y} \dot{\tau}(M, z) \left(-\frac{\mathbf{v}(M, \mathbf{y}) \cdot \mathbf{n}}{c} \right) n[M, \mathbf{y}] W^{gas}[M, \mathbf{r} - \mathbf{y}] \right) \\ &= \int_0^{r_{lss}} dr \int dM \times \\ &\left[\left(\dot{\tau}(M, z) \left(-\frac{\mathbf{v}(M) \cdot \mathbf{n}}{c} \right) n[M] \right) \star W^{gas}[M, z] \right] [\mathbf{r}]. \end{aligned} \quad (18)$$

Note that central optical depth and the window function have an intrinsic dependence on redshift. This is due to the fact that clusters formed at higher redshift tend to be more concentrated. The symbol \star denotes here convolution in real space.

4.3. The all sky correlation function and power spectrum of the kSZ effect

If two different lines of sight are now combined to estimate the angular correlation function, then one obtains that

$$\begin{aligned} \left\langle \frac{\Delta T_{kSZ}}{T_0}[\mathbf{n}_1] \frac{\Delta T_{kSZ}}{T_0}[\mathbf{n}_2] \right\rangle &\propto \\ \left\langle n(M_1, \mathbf{r}_1) \left(\mathbf{v}(M_1, \mathbf{r}_1) \cdot \mathbf{n}_1 \right) n(M_2, \mathbf{r}_2) \left(\mathbf{v}(M_2, \mathbf{r}_2) \cdot \mathbf{n}_2 \right) \right\rangle. \end{aligned} \quad (19)$$

Next we plug eq.(16) and make use of the Cumulant Expansion Theorem. We must note as well that Poissonian fluctuations will be assumed to be independent of δ , and that for Gaussian statistics, the 3- and 4-point functions are zero, just as $\langle \mathbf{v} \rangle$ and $\langle \delta \rangle$. Therefore we are left with a sum of products of 2-point functions of the form

$$\begin{aligned} &\bar{n}(M_1, z_1) \sigma_{vv}^2(M_1, z_1) + \\ &\bar{n}(M_1, z_1) \bar{n}(M_2, z_2) \left\langle \left(\mathbf{v}(M_1, \mathbf{r}_1) \cdot \mathbf{n}_1 \right) \left(\mathbf{v}(M_2, \mathbf{r}_2) \cdot \mathbf{n}_2 \right) \right\rangle + \\ &\left. \frac{\partial \bar{n}(M_1, z_1)}{\partial \delta} \right|_{\delta=0} \left. \frac{\partial \bar{n}(M_2, z_2)}{\partial \delta} \right|_{\delta=0} \times \\ &\left[\langle \delta(\mathbf{r}_1) \delta(\mathbf{r}_2) \rangle \left\langle \left(\mathbf{v}(M_1, \mathbf{r}_1) \cdot \mathbf{n}_1 \right) \left(\mathbf{v}(M_2, \mathbf{r}_2) \cdot \mathbf{n}_2 \right) \right\rangle + \right. \\ &\left\langle \delta(\mathbf{r}_1) \left(\mathbf{v}(M_2, \mathbf{r}_2) \cdot \mathbf{n}_2 \right) \right\rangle \left\langle \delta(\mathbf{r}_2) \left(\mathbf{v}(M_1, \mathbf{r}_1) \cdot \mathbf{n}_1 \right) \right\rangle + \\ &\left. \left\langle \delta(\mathbf{r}_1) \left(\mathbf{v}(M_1, \mathbf{r}_1) \cdot \mathbf{n}_1 \right) \right\rangle \left\langle \delta(\mathbf{r}_2) \left(\mathbf{v}(M_2, \mathbf{r}_2) \cdot \mathbf{n}_2 \right) \right\rangle \right]. \end{aligned} \quad (20)$$

Note that the last term is a constant. We refer again to Appendix A where the cross terms $\langle \delta(\mathbf{v} \cdot \mathbf{n}) \rangle$ are studied. In Appendix C we provide a explicit computation of the power spectra arising from each of the terms considered in eq.(20). Since the last term introduces no anisotropy, the kSZ power spectrum is the sum of four contributions: a Poisson term (*Poisson*), a term proportional to the velocity-velocity correlation (*vv* term), a term proportional to the product of the velocity-velocity correlation and the density-density correlation (*vv-dd* term), and a term proportional to the density-velocity squared (*dv-vd* term). Therefore,

$$C_l = C_l^P + C_l^{vv} + C_l^{dd-vv} + C_l^{dv-vd}. \quad (21)$$

Fig.(4) displays each of the terms in eq.(21): the thick solid line is the Poisson term, whereas the thick dashed line corresponds to the *vv* term. Although the latter decreases rapidly with increasing l , at the large scales it dominates over all other terms, reflecting the presence of the local bulk flow. In an attempt to simplify the expressions for these two terms given in Appendix C, we have found the approximate integral

$$C_l^P \approx \int dz \frac{dV(z)}{dz} dM \bar{n}(M, z) \sigma_{vv}^2(M, z) \frac{|y_l(M, z)|^2}{\pi} \quad (22)$$

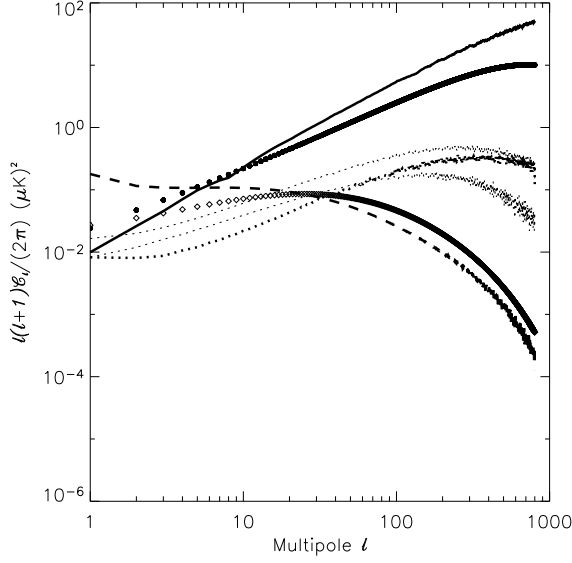


FIG. 4.— Different components of the all-sky kSZ power spectra: the thick solid line shows the Poisson term, which dominates over the other terms except in the low l limit. In this large scale range, the vv generated by the local bulk flow is the one introducing most power, (dashed line). Filled circles and diamonds show semi-analytical approximations for these two *Poisson* and vv , respectively (see eqs.(22,23)). Of lower amplitude, the thick dotted line shows the sum of the $dd-vv$ and the $dv-vd$ terms, (thin dotted lines, note that the latter is negative).

for the Poisson term, and

$$C_l^{vv} \approx \int dz \frac{dV(z)}{dz} P_{vv} \left(z, k = \frac{l}{r(z)} \right) \times \left[\int dM \frac{1}{4\pi} \bar{n}(M, z) |y_l(M, z)|^2 \right] \quad (23)$$

for the vv term. $y_l(M, z)$ is the Fourier transform of the cluster profile in the sphere,

$$y_l = \left(\sqrt{2\pi} \theta_v \right)^2 \exp -l(l+1)\theta_v^2/2, \quad (24)$$

and $P_{vv}(k, z)$ is the k and z dependent velocity power spectrum. θ_v is the angular size of the cluster virial radius. Filled circles for the Poisson term and diamonds for the vv term provide a comparison of these approximations with the exact integrals. Although the amplitudes and slopes are not too dissimilar, the approximated vv term is particularly inaccurate at large angular scales ($l < 10$). The approximation for the Poissonian term seems to predict a somewhat correct amplitude at low l , but a shallower slope, which translates into a smaller amplitude at high multipoles.

The $dd-vv$ and $dv-vd$ terms are shown by the thin dotted lines. We must remark that the $dv-vd$ term is negative, and we are plotting its absolute value. The sum of both is given by the thick dotted line. The sum of these two terms is particularly hard to detect, since it never dominates, not at large scales (it is about a factor of 20 below the vv term), nor at small scales, where it is well below the Poisson term.

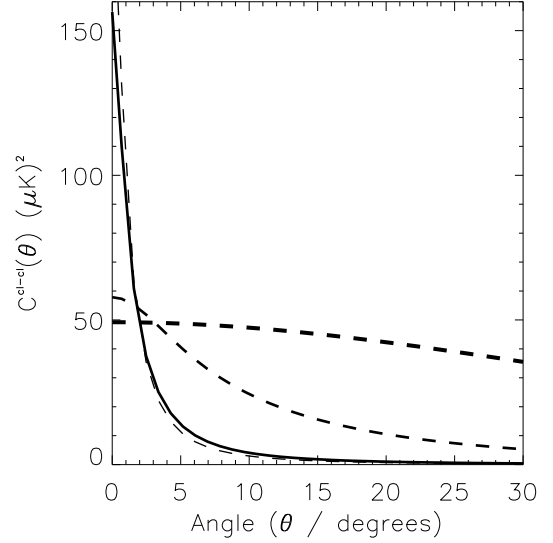


FIG. 5.— Cluster-cluster kSZ correlation functions for a sample of clusters with masses above $2 \times 10^{14} M_\odot$. When forming cluster pairs we require pair constituents to be at similar redshifts. If we consider all redshifts simultaneously, we obtain the solid line. The dashed lines correspond to *differential*-in-redshift cluster-cluster correlation functions: the thick dashed line considers only clusters around $z \sim 0.01$, whereas the intermediate dashed line corresponds to $z \sim 0.1$ and the thin dashed line to $z \sim 1$.

4.4. The cluster-cluster kSZ correlation function

Future high resolution multi frequency CMB experiments like ACT or SPT can provide kSZ estimates on those regions of the sky where clusters of galaxies have been identified via tSZ. Therefore one could attempt to measure the velocities correlation function by computing the kSZ correlation function in this *restricted* set of pixels:

$$C_{kSZ}^{cl-cl}(\theta) = \sum_{i_1, i_2} \sum_{j_1, j_2} \tau(M_{i_1}, z_{j_1}) \tau(M_{i_2}, z_{j_2}) \times \left\langle \frac{1}{c^2} \left(\mathbf{v}(M_{i_1}, z_{j_1}) \cdot \mathbf{n}_1 \right) \left(\mathbf{v}(M_{i_2}, z_{j_2}) \cdot \mathbf{n}_2 \right) \right\rangle. \quad (25)$$

Since the signal comes from clusters which velocities are correlated, we should consider pairs close in redshift. The solid line in Fig.(5) shows the correlation function to be measured from *all* galaxy clusters from $z = 0$ upto $z = 4$ more massive than $2 \times 10^{14} h^{-1} M_\odot$, according to the standard Λ CDM cosmology and the Sheth-Tormen mass function. Members of the cluster pairs must be within $\Delta z = 0.01$. Since the kSZ amplitude per cluster is typically of few tens of microKelvin, the zero-lag correlation function can be as high as $\sim 150 (\mu\text{K})^2$, and drops to one half of this value at $\theta \sim 2^\circ - 3^\circ$. The thick dashed line shows the correlation function for clusters located at $z \simeq 0.01$. As the redshift increases ($z \simeq 0.1$ medium thickness dashed line; $z \simeq 1$, thin dashed line), the amplitude at zero lag increases (clusters are more concentrated) and the correlation angle decreases. The solid line shows the redshift-integrated cluster-cluster correlation function: the signal is dominated by high redshift clusters, more concentrated and more numerous per unit solid angle.

Diaferio, Sunyaev & Nusser (2000) pointed out a potentially important non-linear aspect that is not included in our

modeling: in very massive superclusters, the kSZ effect shows typically a dipolar pattern, plausibly caused by the encounter of two opposite bulk flows at their common attractor's position. Since our model predicts no dipolar pattern at scales of a few degrees, such scenario is not accounted for by our approach. Hence, in a realistic application the core of such overdense regions should be excised from the analyses. Such massive structures however are very rare and form at very late epochs, and their exclusion should not compromise the analysis presented here.

5. CAN THE KSZ EFFECT BE MEASURED?

In this section we outline two different procedures to extract the kSZ signal from future high-resolution and high-sensitivity CMB experiments. The procedures presented here may be sub-optimal but our aim is to quantify the relative importance of difference sources of error and to roughly forecast the expected signal to noise for those experiments. We defer the development of an optimal procedure to future work. We shall try to extract the kSZ signal in a statistical sense: while previous works (e.g., Aghanim et al. (2004)) have addressed the difficulty of separating the kSZ effect from potential contaminants (tSZ, radio-source emission, infrared galaxies, CMB, etc) in a given cluster, our approach will consist on combining the signal coming from subsets of clusters in such a way that the contribution of the noise sources averages out. As we shall see, the success of this procedure will rely on the precision to which the *average* properties of the potential contaminants are known.

The first approach, which we shall refer to as method (a), is based on measurements of the kSZ flux and its redshift evolution. Its sensitivity to cosmology increases with redshift, and, for this reason it is suited for “deep and narrow” survey strategies. Here we will use ACT’s specifications. Our second approach (method (b)) uses the ratio of kSZ and tSZ induced temperature anisotropies. This ratio is particularly sensitive to w at $z \lesssim 0.8$ and since cosmic variance for the peculiar velocity field is more important at low redshifts, this method is more suitable for “wide and shallow” survey strategies. Here we will use a survey with specifications similar to those of ACT, but covering 4,000 square degrees and thus with higher noise. These specifications are not too dissimilar from those of SPT, assuming that accurate photometric redshifts can be obtained for all SPT clusters.

5.1. Probing the kSZ flux at high redshift

In what follows, we shall use specifications for ACT one year data (Gaussian beam with FWHM equal to 2 arcmins, noise amplitude lower than $2 \mu\text{K}$ per beam, and a clean scanned area of 400 square degrees). ACT observes in three bands: 145, 220 and 250 GHz. We will concentrate on the 220 GHz channel, although some knowledge will be assumed to be inferred from the other bands. For instance, the 250 GHz channel will be very useful to estimate the level of infrared-galaxy emission at lower frequencies. Likewise, the 145 GHz channel should be critical when characterizing the tSZ flux from each cluster. For simplicity, we will concentrate on the variance of the kSZ signal, but it is easy to estimate the kSZ angular correlation function introduced in subsection 4.4.

The strip covered by ACT should also be surveyed by

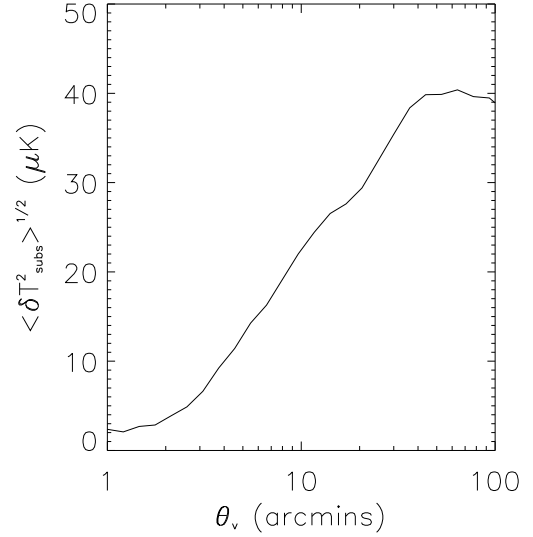


FIG. 6.— Typical amplitude of CMB residuals remaining after attempting to approximate the CMB average within a circular patch of angular radius θ_v (given in abscissas) by the CMB average computed within a ring surrounding the patch of width 10% the patch radius. For most of clusters located at $z > 0.3$, these residuals will typically be of $3 - 4 \mu\text{K}$ amplitude.

SALT⁵. Cluster detection via tSZ effect will provide targets for optical observations. Alternatively, optical cluster identification should be possible up to $z \sim 1$ from SALT’s multi-band imaging using algorithms such as those developed in Kim et al. (2002); Miller et al. (2005). Hence, a direct comparison can be made with tSZ detected cluster sample. SALT spectroscopic follow up will enable to obtain the cluster redshifts.

The method is as follows:

- For every detected galaxy cluster, we take a patch of radius equal to one projected cluster virial radius. We can use the edge of significant tSZ emission at other frequencies to define this radius. We compute the mean temperature within this patch, and draw a ring surrounding it, of width, say, 10% of the virial radius. We next compute the mean temperature within this ring and subtract it from the mean of the patch. This operation should remove most of the CMB contribution to the average temperature in the patch, but will unavoidably leave some residuals, which will be denoted here as $\delta T_{\text{cmb}}^{\text{res}}$. These residuals will have two different contributions: the first coming from the inaccurate CMB subtraction, the second one being due to instrumental noise residuals,

$$\langle (\delta T_{\text{CMB}}^{\text{res}})^2 \rangle = \langle \delta T_{\text{subs}}^2 \rangle + \frac{N^2}{N_{\text{beams}}}. \quad (26)$$

N_{beams} is the number of beam sizes present in the ring, and N^2 is the instrumental noise variance. If we denote the patch of radius the cluster virial radius as *region 1*, and by *region 2* the ring surrounding it, it can be easily

⁵ SALT’s URL site: <http://www.salt.ac.za/>

proved that the first term in the RHS of the last equation reads

$$\begin{aligned} \langle \delta T_{subs}^2 \rangle &= \frac{1}{(\Delta\Omega_1)^2} \int_{\Delta\Omega_1} \int_{\Delta\Omega_1} d\mathbf{n}_1 d\mathbf{n}_2 C(\mathbf{n}_1, \mathbf{n}_2) + \\ &\quad \frac{1}{(\Delta\Omega_2)^2} \int_{\Delta\Omega_2} \int_{\Delta\Omega_2} d\mathbf{n}_1 d\mathbf{n}_2 C(\mathbf{n}_1, \mathbf{n}_2) - \\ &\quad \frac{2}{\Delta\Omega_1 \Delta\Omega_2} \int_{\Delta\Omega_1} \int_{\Delta\Omega_2} d\mathbf{n}_1 d\mathbf{n}_2 C(\mathbf{n}_1, \mathbf{n}_2). \end{aligned} \quad (27)$$

$\Delta\Omega_1$ and $\Delta\Omega_2$ denote the solid angles of the patch and the ring, respectively, whereas \mathbf{n}_1 and \mathbf{n}_2 denote directions in the sky and $C(\mathbf{n}_1, \mathbf{n}_2)$ is the CMB angular correlation function evaluated at the angle separating the directions \mathbf{n}_1 and \mathbf{n}_2 . The rms fluctuations introduced by this residual are plotted in Fig.(6): although it can be as high as a few tens of microK for nearby clusters subtending 30 – 40 arcmins, their effect reduces to a 3 – 4 μ K for clusters of a few arcmins size, which correspond to most of clusters at $z > 0.3$ to be detected by ACT-like CMB experiments. This contaminant will be dominant over the instrumental noise contribution.

- We assume that, by observing the tSZ amplitudes at 145 GHz and 250 GHz, it is possible to provide an *unbiased* estimate of the mean tSZ contribution to the cluster patch at 220 GHz. After subtracting the tSZ and CMB components estimates, the temperature in the patch corresponding to cluster i can be written as

$$\delta_i = \delta T_{CMB,i}^{res} + \delta T_{tSZ,i} + N + \delta T_{kSZ,i}^{int} + T_{kSZ,i}. \quad (28)$$

$\delta T_{tSZ,i}$ denotes the tSZ residuals *after* subtracting the estimated tSZ amplitude. N accounts for contribution of instrumental noise to the patch average, and $\delta T_{kSZ,i}^{int}$ for the residual contribution of internal velocities. According to Diaferio et al. (2005), we assume a typical rms for internal velocities of one third the bulk flow velocity expected for each cluster, and random orientation (sign); thus we assume $\delta T_{kSZ,i}^{int}$ rms to be 1/3 of the bulk-flow induced kSZ amplitude. The first four quantities in the RHS of eq.(28) have zero mean, hence δ_i is an *unbiased* estimate of the kSZ amplitude in cluster i .

- We now combine estimates of the kSZ coming from *different* clusters in order to estimate the kSZ cluster-cluster correlation function, $\langle T_{kSZ,i} T_{kSZ,j} \rangle$. As mentioned in a previous Section, we are interested in computing this correlation function by considering pairs of clusters of similar redshift. Note that we avoid squaring the kSZ estimate of the same cluster ($i = j$), since residuals would not average out and would introduce a bias in our kSZ variance estimates. Let us assume that the bulk flows occupy a typical scale (named here as *coherence scale*) θ_{coh} on the sky. Within this patch along direction \mathbf{n} , we can sort all clusters in mass and redshift bins. Let I, J, L and M denote the mass bins of clusters in a common redshift range centered at z_l . By building cluster pairs upon all members of these bins, and combining different mass bins, it is possible to compute the

following kSZ variance⁶ estimator at redshift z_l along the direction \mathbf{n} :

$$\tilde{F}_{kSZ,l}^2(\mathbf{n}) \equiv \sum_{I \leq J} \frac{w_{I,J}}{N_{I,J}} \sum_{i,j} (\delta_i \Omega_i) (\delta_j \Omega_j) / \sum_{I \leq J} w_{I,J}. \quad (29)$$

Ω_j stands for the j -th cluster's solid angle. We remark that the kSZ flux depends solely on the cluster's mass and peculiar velocity, and so do our angle-integrated kSZ temperature anisotropies. If we denote by N_I and N_J the number of cluster members in bins I and J , respectively, then the number of cluster pairs that can be formed by combining these two mass bins is given by $N_{I,J}$; $N_{I,J} = N_I N_J$ if $I \neq J$ and $N_{I,J} = N_I(N_I - 1)/2$ for the same bin ($I = J$). The indexes i and j run for individual cluster members in each mass bin. $w_{I,J}$ is a weight factor, which we define as

$$\begin{aligned} w_{I,J} &\equiv \frac{N_I N_J}{\sigma_I^2 \sigma_J^2} = \\ &\quad \frac{N_I}{\Omega_I^2 [\langle \delta T_{CMB}^{res} \rangle^2 + \langle \delta T_{tSZ} \rangle^2 + \langle (\delta T_{kSZ}^{int})^2 \rangle + N^2]_I} \times \\ &\quad \frac{N_J}{\Omega_J^2 [\langle \delta T_{CMB}^{res} \rangle^2 + \langle \delta T_{tSZ} \rangle^2 + \langle (\delta T_{kSZ}^{int})^2 \rangle + N^2]_J}, \end{aligned} \quad (30)$$

with the subscripts I and J evaluating the brackets in the corresponding mass bins. The estimator of eq.(29) provides a weighted measurement of the kSZ variance,

$$\langle \tilde{F}_{kSZ,l}^2(\mathbf{n}) \rangle = \frac{\sum_{I \leq J} w_{I,J} (F_{kSZ,I} F_{kSZ,J})}{\sum_{I \leq J} w_{I,J}}, \quad (31)$$

with $F_{kSZ,I}$ the expected kSZ amplitude at redshift z_l and mass equal to that corresponding to bin I . Its formal error is given by

$$\begin{aligned} \Delta^2[\tilde{F}_{kSZ,l}^2(\mathbf{n})] &= \\ &2 \times \left[\frac{\sum_{I \leq J} w_{I,J} (F_{kSZ,I} F_{kSZ,J})}{\sum_{I \leq J} w_{I,J}} \right]^2 + \\ &\quad \sum_{I,J,L} w_{I,J,L} (F_{kSZ,I} F_{kSZ,L}) / \left(\sum_{I \leq J} w_{I,J} \right)^2 + \\ &\quad \sum_{I,J,M} w_{I,J,M} (F_{kSZ,I} F_{kSZ,M}) / \left(\sum_{I \leq J} w_{I,J} \right)^2 + \\ &\quad 1 / \sum_{I \leq J} w_{I,J}, \end{aligned} \quad (32)$$

where $w_{I,J,L} \equiv w_{I,J} N_L / \sigma_L^2$. Note that the first term in the RHS of this equation is not sensitive to the number of clusters within the coherence patch. Such term, containing the squared kSZ expectations for mass bins I and J , is associated to the (assumed) intrinsic Gaussian nature of the kSZ fluctuations, and it corresponds to the *cosmic variance* contribution. It will thus scale like the inverse of the survey area when different

⁶ We integrate temperature fluctuations in the cluster's area, obtaining a quantity of units μ K-strad. This integrated temperature fluctuations are essentially proportional to *flux* fluctuations, and for this reason they will be denoted by \tilde{F}_{kSZ} . One must keep in mind, however, that their units are not Janskys, but microKelvin \times stereoradian.

coherence patches are combined in the analysis. The forth term is exclusively due to observational errors, whereas the second and third terms are hybrid: they show contributions from both the intrinsic uncertainty of the velocity field and observational errors. If N_b denotes the number of mass bins, and we take the weights, the cluster number and the F_{kSZ} equal for all mass bins ($\sigma_I = \sigma$, $N_I = N$ and $F_{kSZ,I,I} = F_{kSZ,I}$ for every mass bin I), then it can easily be proved that the forth term scales roughly as $\sigma^4/N^2/(N_b(N_b+1))$, that is, the squared variance expected for each cluster over the total number of pairs that can be formed. The second and third terms, in this limit, yield $\sigma^2 F_{kSZ,I}^2/(N(N_b+1))$, which scales inversely to the number of clusters. In our case, our kSZ flux estimates will be limited by the cosmic variance term. On the other hand, because of having very few objects, we considered one mass bin only.

- Finally, we combine estimates from the $N_{coh} \simeq 4\pi f_{sky}/\theta_{coh}^2$ different projected coherent regions in the sky, where f_{sky} is the fraction of the sky covered by the CMB experiment, yielding

$$\tilde{F}_{kSZ,I}^2 \equiv \sum_{\mathbf{n}} \frac{\tilde{F}_{kSZ,I}^2(\mathbf{n})}{\Delta^2[\tilde{F}_{kSZ,I}^2(\mathbf{n})]} \bigg/ \sum_{\mathbf{n}} \frac{1}{\Delta^2[\tilde{F}_{kSZ,I}^2(\mathbf{n})]}, \quad (33)$$

with an uncertainty

$$\Delta^2[\tilde{F}_{kSZ,I}^2] = 1 \bigg/ \sum_{\mathbf{n}} \frac{1}{\Delta^2[\tilde{F}_{kSZ,I}^2(\mathbf{n})]}. \quad (34)$$

Note that the size of the coherent patch must depend of redshift: a bulk flow extending up to $20 h^{-1}\text{Mpc}$ at $z=1$ subtends a degree on the sky, whereas if it is at $z \simeq 0.05$ then it subtends around 8 degrees.

We take the effective noise N to have a typical amplitude of $5 \mu\text{K}$ per beam⁷, and it accounts for both instrumental noise and the confusion noise associated to unresolved sources. δT_{CMB}^{res} is computed as stated in eq.(27), and contributes typically with a few microK. Regarding the tSZ residuals, δT_{tSZ} contains the contribution coming from relativistic tSZ corrections, and power leakage associated to the finite spectral width of the detectors. We conservatively assume that the amplitude of these residuals (remaining after the tSZ subtraction) is typically the non-relativistic tSZ temperature increment expected at 222 GHz. We approximate the beam as a Gaussian of FWHM equal to 2 arcmins, and take 400 square degrees ($f_{sky} \simeq 10^{-2}$) as the clean sky region covered by ACT. ACT's sensitivity limit is set to cluster above $2 \times 10^{14} h^{-1} M_\odot$, and the total number of clusters above this threshold predicted in this region of the sky by our Sheth-Tormen mass function is roughly 4,400. However, for this analysis we only use relatively bright and big clusters: the product of their angular size and tSZ temperature decrement at 145 GHz must be bigger than $160 \mu\text{K arcmin}^2$, and this requirement decreases considerably the amount of available clusters.

As a result of this section, in Fig.(7) we show our expectations of ACT's sensitivity on the kSZ variance when all clusters are grouped in the redshift bins $z_i^{band} \equiv [0.02, 0.4, 0.8,$

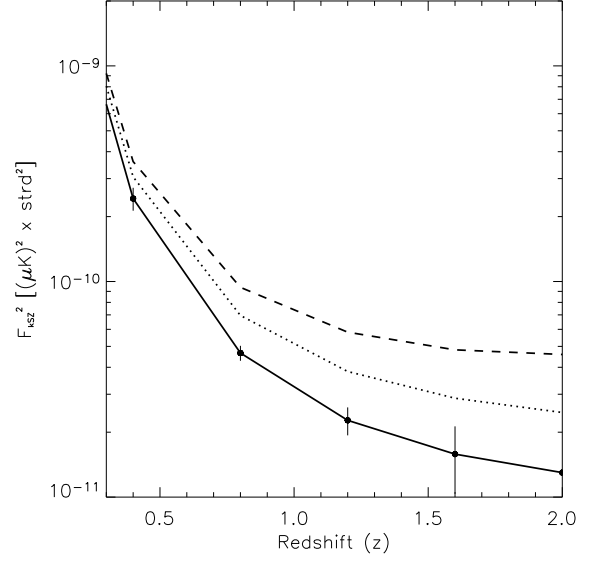


FIG. 7.— Expected amplitude of the squared kSZ flux for ACT, after grouping all cluster in six redshift bins. The solid line corresponds to a ΛCDM . The dotted and the dashed lines display the kSZ variances for universes with Dark Energy components having w equal to -0.6 and $-1/3$, respectively

1.2, 1.6, 2.0]. Solid, dotted and dashed lines correspond to a ΛCDM model ($\Omega_m = 0.3, \Omega_\Lambda = 0.7$), a flat universe with dark energy equation of state $w = -0.6$, and $w = -1/3$, respectively. We report error bars for the ΛCDM model: we drop the first point at $z = 0.02$ (which is dominated by cosmic variance) and focus in the high redshift range: the signal-to-noise ratio shows a maximum at $z=0.8$, and beyond this redshift the error bars start to increase due to the lack of massive clusters.

5.2. The kSZ/tSZ ratio \mathcal{R}

In this subsection, we address the study of the ratio of the kSZ and tSZ effects. When referring to temperature anisotropies, the kSZ and tSZ effects are integrals weighted by the cluster electron density along the cluster diameter, and are sensitive to the size and/or the concentration parameter of these objects. The ratio of the kSZ and the tSZ, however, should cancel these dependencies out to great extent, and provide a cleaner view of the cluster's temperature and peculiar velocity.

Following our cluster model, we investigate the behaviour of the statistic $\mathcal{R} \equiv \delta T_{kSZ}/\delta T_{tSZ}$ in the cluster population. If the evolution of the cluster temperature is well described by the spherical collapse model, we shall find then that \mathcal{R} should be a good estimator of the dark energy equation of state w at recent epochs. But since cosmic variance becomes important at low redshifts (smaller volume for a given solid angle), in this case we shall compute our expectations for an experiment with sky coverage close to $f_{sky} = 0.1$ (4,000 square degrees). To compensate for the wider survey area we assume a noise of $10 \mu\text{K}$ per arcminute squared and that clusters up to $z = 0.8$ can be detected and resolved. We assume that the frequency coverage enables contaminant subtraction and extraction of clusters tSZ signal. We also assume that follow up observations will yield redshift for all observed clusters.

⁷ The noise level for ACT is expected to be $\lesssim 2 \mu\text{K}$ per beam.

These specifications are not too dissimilar to those of the SPT telescope when combined with photometric follow up.

We shall see that these are precisely the requirements needed to obtain cosmological information from \mathcal{R} . However, since in this case the kSZ signal is divided by the tSZ temperature decrement (measured at say, 145 GHz), we must be very careful with the noise contribution to the denominator of \mathcal{R} . Our approach will be to conservatively consider only clusters whose integrated tSZ temperature decrements are larger than $160 \mu\text{K-arcmin}^2$ at 145 GHz. This implies that tSZ errors will be typically 5% – 10% of the estimated tSZ temperature decrement, and that they can be treated perturbatively as errors in the kSZ estimation in the numerator. Therefore, our model for the estimation of \mathcal{R} in a single cluster will be given by:

$$r_i = \frac{\delta T_{\text{CMB},i}^{\text{res}} + \delta T_{\text{tSZ},i} + N + \delta T_{\text{kSZ},i}^{\text{int}} + \epsilon T_{\text{kSZ},i} + T_{\text{kSZ},i}}{T_{\text{tSZ},i}}. \quad (35)$$

Most of the terms of this equation are defined exactly as in eq.(28). The only new term is $\epsilon T_{\text{kSZ},i}$, which accounts for the extra error introduced by the uncertainty in the denominator, $T_{\text{tSZ},i}$. Here $T_{\text{tSZ},i}$ is the absolute value of the tSZ decrement of the cluster at 145 GHz and ϵ was taken to be a normal random variable of rms 0.05 (5% error in $T_{\text{tSZ},i}$ which reflects into 5% error in $T_{\text{kSZ},i}$). We neglect the correlation of the errors in $T_{\text{tSZ},i}$ with those of $T_{\text{kSZ},i}$ and take ϵ independent of the other noise sources.

We now write the analogue to eq.(29) as

$$\tilde{\mathcal{R}}_l(\mathbf{n}) \equiv \sum_{I \leq J} \frac{w_{I,J}}{N_{I,J}} \sum_{i,j} r_i r_j / \sum_{I \leq J} w_{I,J}, \quad (36)$$

where the weights are defined as

$$w_{I,J} \equiv \frac{N_I N_J}{\sigma_I^2 \sigma_J^2} = \frac{N_I T_{\text{tSZ},I}^2}{[\langle \delta T_{\text{CMB}}^{\text{res}} \rangle^2 + \langle \delta T_{\text{tSZ}}^2 \rangle + \langle (\delta T_{\text{kSZ}}^{\text{int}})^2 \rangle + \epsilon^2 T_{\text{kSZ},I}^2 + N^2]_I} \times \frac{N_J T_{\text{tSZ},J}^2}{[\langle (\delta T_{\text{CMB}}^{\text{res}})^2 \rangle + \langle \delta T_{\text{tSZ}}^2 \rangle + \langle (\delta T_{\text{kSZ}}^{\text{int}})^2 \rangle + \epsilon^2 T_{\text{kSZ},J}^2 + N^2]_J}. \quad (37)$$

The estimate of $\tilde{\mathcal{R}}_l(\mathbf{n})$ in a redshift band z_l and direction \mathbf{n} , together with its uncertainty $\Delta^2[\tilde{\mathcal{R}}_l(\mathbf{n})]$ can be obtained from eqs.(31,32) by simply replacing $\tilde{F}_{\text{kSZ},l}^2(\mathbf{n})$ by $\tilde{\mathcal{R}}_l(\mathbf{n})$. Similarly the expressions for $\tilde{\mathcal{R}}_l$ and $\Delta^2[\tilde{\mathcal{R}}_l]$ can be obtained from eqs.(33,34).

In Fig.(8) we plot the ratio \mathcal{R} at different redshifts as it would be seen by an experiment like SPT. As before, we have assumed that only clusters above $2 \times 10^{14} h^{-1} M_\odot$ can be seen, and grouped all clusters in the redshift bins $z_l^{\text{band}} \equiv [0.02, 0.4, 0.8, 1.2, 1.6, 2.0]$. The lines refer to the same cosmological models as in Fig.(7). Note the similarity of this plot and Fig.(1). We see that \mathcal{R} is sensitive to cosmology at much lower redshifts ($z \lesssim 0.8$) than F_{kSZ} , and for the sensitivity analysis following in the next Section we have only used the first three redshift bins.

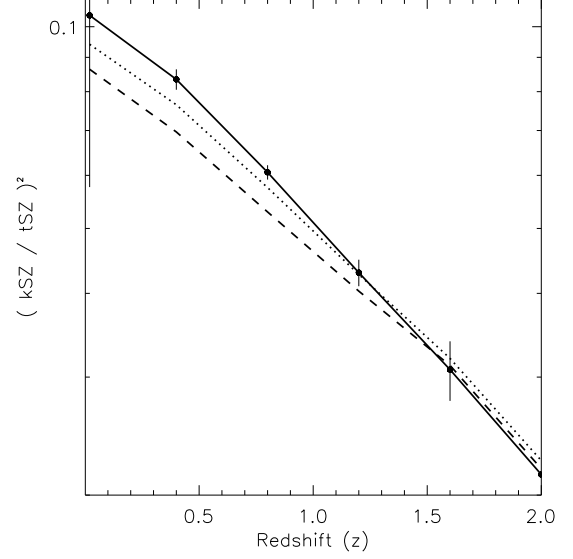


FIG. 8.— Expected kSZ/tSZ ratio \mathcal{R} as measured by SPT for six redshift bins. The solid line corresponds to a Λ CDM model while the dotted and the dashed lines are for flat models with w equal to -0.6 and -1/3, respectively.

6. KSZ SENSITIVITY TO MEASURING COSMOLOGICAL PARAMETERS

We can now explore the dependence of the two statistics introduced in the previous Section on cosmological parameters. We define the χ^2 as

$$\chi^2 \equiv \sum_l \frac{(\tilde{Q}_{\text{kSZ},l}^2 - Q_{\text{kSZ},l}^2)^2}{\Delta^2[Q_{\text{kSZ},l}^2]}, \quad (38)$$

where $Q_{\text{kSZ},l}^2$ can either refer to the angle-averaged kSZ anisotropy (F) or the kSZ/tSZ ratio (\mathcal{R}). The likelihood is thus $\mathcal{L} \propto \exp(-\frac{1}{2}\chi^2)$. We estimate errors using the Fisher matrix approach. In principle the parameters that enter in the analysis are Ω_m , w , the fraction of cluster mass in the intra cluster medium f_{ICM} , the present-day normalization of the matter density fluctuations σ_8 and the reduce Hubble constant h . In practice both methods are non sensitive to f_{ICM} , σ_8 and h separately for a fixed number of detected clusters, but on their combination in the form of an overall amplitude of the kSZ signal, which we shall assign to an amplitude parameter A alone.

We assume that A is redshift-independent (or that its scaling in redshift can be constrained) and consider a 20% uncertainty in this normalization, owing to 10% uncertainty in σ_8 , f_{ICM} and h each, over which we marginalize. We remark, however, that our results will be practically insensitive to the uncertainty on A . In Fig.(9) we show the resulting constraints in the Ω_m - w plane. Clearly, the F_{kSZ} method is more sensitive to w than \mathcal{R} , and their directions of degeneracy are also different, but both distinct to the directions of degeneracy corresponding to estimators based upon Large Scale Structure. Indeed, these estimators are restricted to the low redshift universe, and hence their sensitivity on w is very limited, giving rise to degeneracy direction almost parallel to the w axis, (see, e.g., Fig (11) in Eisenstein et al.

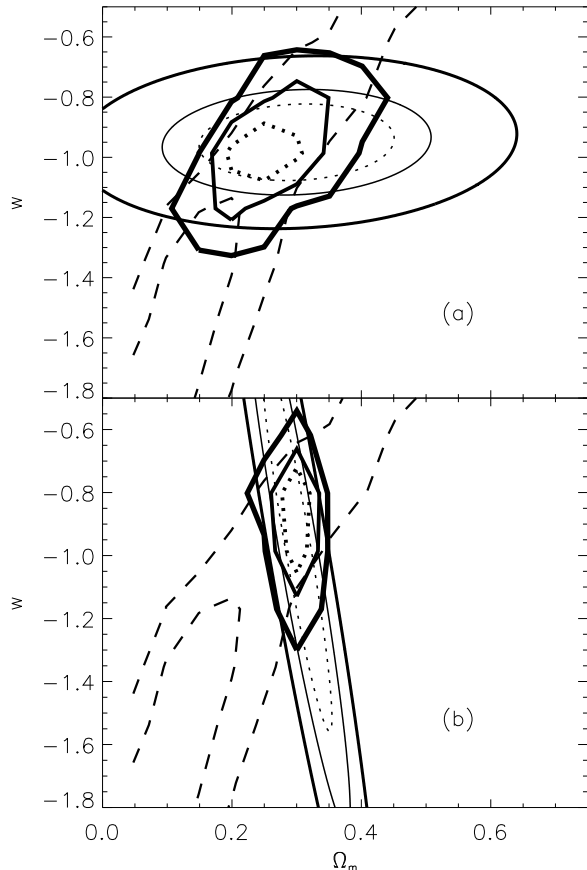


FIG. 9.— Contour plots showing the 1 and 2- σ joint confidence region (solid line) and the 1- σ marginalized (dotted line) in the $\Omega_m - w$ plane for the F_{kSZ}^2 (method (a)) and \mathcal{R}^2 (method (b)) estimations. Method (a) applied to ACT (top) with CMB (WMAP 1st year) priors (dashed lines) yields a $\sim 8\%$ error on w . This error would drop below 5% if ACT covers 1,000 square degrees. Method (b) on a SPT-like survey gives a $\sim 12\%$ error on w after imposing the prior from WMAP’s 1st year data.

(2005) or Fig. (13) in Tegmark et al. (2004)). The constraint on w , marginalized over Ω_m , is $\sim 12\%$ for F_{kSZ} and $\sim 60\%$ for \mathcal{R} . As the degeneracy direction in each case is different to that corresponding to CMB temperature measurements, a combination with analyses of CMB temperature data can break the degeneracy. When considering WMAP first year data, the marginalised error on w reduces to $\sim 8\%$, $\sim 12\%$, for F_{kSZ} and \mathcal{R} methods, respectively (thick dotted lines). As pointed above, these errors are dominated by the cosmic variance term present in eq.(32). Therefore, by increasing the sky covered by the experiments, those errors should decrease as $\propto 1/\sqrt{f_{sky}}$.

These results have been obtained after using a ST mass function, and assuming that the cluster density was uniform (i.e., we have considered no biases). The error amplitudes and the orientation of the ellipses in Fig (9) depend strongly on the number of cluster pairs that can be formed in each redshift bin, particularly at the high z end. If the actual sensitivity of future CMB experiments is such that the lower limit on detectable clusters can be relaxed (we believe the limit $2 \times 10^{14} h^{-1} M_\odot$ to be very conservative for ACT’s

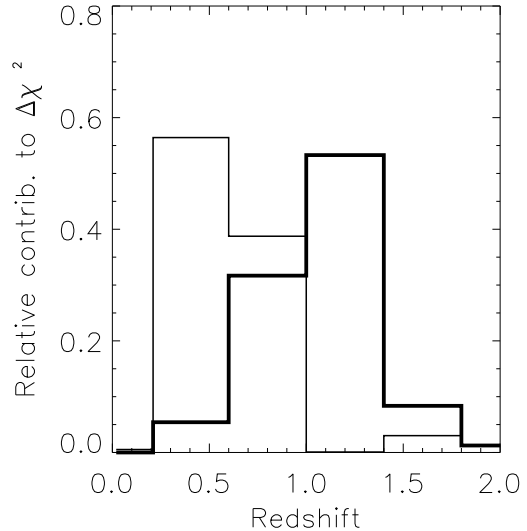


FIG. 10.— Differential redshift contribution to the change in χ^2 when probing models with different w : approach a) is more sensitive to higher redshifts (thick line), method b) to lower redshifts (thin line).

noise level), then the resulting number of cluster pairs that can be formed would increase considerably, and this would reflect on an increased sensitivity to w .

We note that, a priori, the two methods are nicely complementary in their redshift ranges sensitive to w as shown in Fig.(10): we find that the F_{kSZ}^2 estimation (method a) thick histogram) is sensitive to w at high redshifts ($z > 0.5$), whereas \mathcal{R} for different dark energy models differs at low redshift and converges at $z \approx 1$: the sensitivity of this method is localised mainly at low redshift (thin histogram).

After parametrising the evolution of w as $w(a) = w_0 + w_a(1 - a)$, with $a = 1/(1+z)$ the scale factor, we conduct a Fisher matrix analysis considering the parameter set $[\Omega_m, w_0, f_{ICM}, w_a]$ for the F_{kSZ}^2 method. The marginalization in the $w_0 - w_a$ plane is given in Fig.(11), which shows this method should have some residual sensitivity on w_a (a typical error of ~ 1.75 in w_a). Note that this error should be improved further after combining the two methods proposed here, provided that they are sensitive to different redshift ranges.

7. CONCLUSIONS

We have studied bulk flows in the large scale structure in the context of the kSZ effect and future high-sensitivity and high-resolution CMB experiments like ACT. Since the kSZ effect is only sensitive to the projected peculiar velocities of electron clouds, we have focussed our analysis on the angular correlation of radial peculiar velocities in galaxy clusters. We have provided an analytical expression for the angular correlation function of projected peculiar velocities in the linear regime, and interpreted it in the context of local and distant bulk flows. We have also presented an expression for the power spectrum of projected linear peculiar velocities.

We have investigated in which redshift and for which

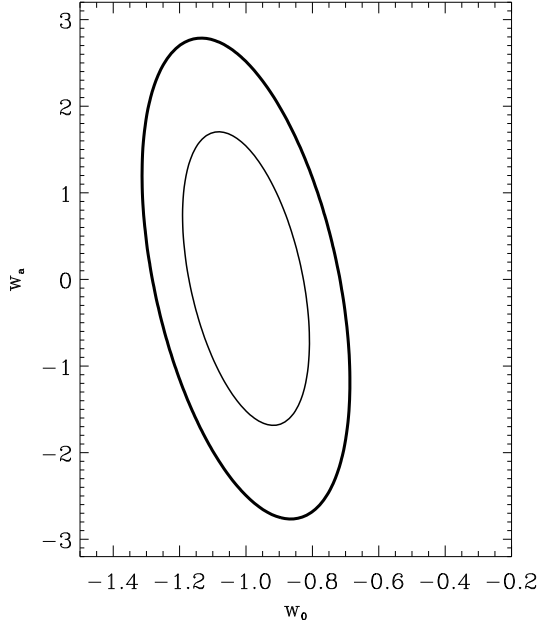


FIG. 11.— Marginalisation in the w_0 - w_a plane for the ACT-like experiment. w_a expresses the variation of w , which is parametrised as $w(a) = w_0 + w_a(1 - a)$, with a the scale factor. Contours correspond to 1 & 2- σ joint confidence regions.

cluster mass ranges large-scale bulk flows should be more easily detectable in future kSZ surveys, and computed the overall effect of the entire galaxy cluster population on the CMB sky. We have shown that the main contribution comes from Poissonian/random fluctuations of the number of clusters along the line of sight, especially at small angular scales. However, we find that the local bulk flow generates a signal which should be dominant at the very large angular scales of the quadrupole and octupole. Other terms associated to the coupling of velocity with density fluctuations give smaller contributions. We have calculated the kSZ signal for the cluster sample accessible by forthcoming experiments, and considered different sources of contamination which may

limit our capacity to distinguish the kSZ signal from other components.

We have presented two approaches to measure the kSZ signal and exploit its dependence on cosmological parameters such as the equation of state of dark energy (w). The first method is based on measurements of the kSZ flux and its redshift evolution. Its sensitivity to cosmology increases with redshift. For this reason it is suited for “deep and narrow” survey strategies. A data set such as that provided by ACT 2 year observations with SALT follow up is well suited for an application of this method. ACT can detect the kSZ signal with a $S/N \sim 12$ at $z \sim 1$.

The second approach uses the ratio of kSZ and tSZ-induced temperature anisotropies. The cosmology-dependence is strongest at low redshift and hence this method is suitable for “wide and shallow” survey strategies. In this case we have considered an ACT-like experiment with larger sky coverage (1/10 of the sky) and increased instrumental noise. These are specifications similar to those of SPT with at least three frequency bands and combined with redshift determinations of the detected clusters. In this case the kSZ effect can be detected with a S/N of ~ 30 .

These methods can yield constraints on cosmological parameters, in particular can constrain the equation of state for dark energy at the 10% level. The two methods are nicely complementary as they measure dark energy in different redshift ranges, opening up the possibility to constrain dark energy redshift evolution.

ACKNOWLEDGMENTS

We are indebted to Ravi Sheth for help and enlightening discussions on cluster spatial correlations and non linear velocities. LV thanks Mark Devlin for discussions. We thank Simon Dedeo for comments and discussions. This research is supported in part by grant NSF AST-0408698 to the Atacama Cosmology Telescope. CHM and LV are supported by NASA grants ADP03-0000-0092 and ADP04-0000-0093. The work of RJ is supported by NSF grants AST0206031, AST-0408698, PIRE-0507768 and NASA grant NNG05GG01G. DNS is supported by NSF grants PIRE-0507768 and through the NASA ATP programs and the WMAP project.

APPENDIX APPENDIX A

Coupling the linear density and velocity fields

In linear theory, the density contrast $\delta(\mathbf{x}) \equiv (\rho(\mathbf{x}) - \bar{\rho})/\bar{\rho}$ is still much smaller than unity. This allows linearising the evolution equations and neglecting all non-linear orders, which makes the evolution of each Fourier mode $\delta_{\mathbf{k}}$ is independent from the other modes.

In a Friedmann Robertson Walker (FRW) universe, the perturbed continuity equation reads

$$\frac{\partial \delta(\mathbf{x})}{\partial t} + \frac{\nabla \mathbf{v}(\mathbf{x})}{a} = 0, \quad (\text{A1})$$

which can be re-written in Fourier domain as

$$\frac{\partial \delta_{\mathbf{k}}}{\partial t} = -\frac{i}{a} \mathbf{k} \cdot \mathbf{v}_{\mathbf{k}}, \quad (\text{A2})$$

with $a = 1/(1+z)$ the scale factor. Throughout this paper, the velocities are *proper* peculiar velocities. We must note that the expansion of the velocities in terms of its Fourier modes is given by

$$\mathbf{v}(\mathbf{x}) = \int \frac{d\mathbf{k}}{(2\pi)^3} \mathbf{v}_{\mathbf{k}} \exp(-i\mathbf{k}\mathbf{x}), \quad (\text{A3})$$

and that, due to isotropy, the different components are independent. The statistical properties of each of them must be, however, identical.

Coming back to eq.(A2), if we denote by $\mathcal{D}_\delta(z)$ the growth factor of the density perturbations, then we can express the component of $\mathbf{v}_{\mathbf{k}}$ parallel to \mathbf{k} (denoted here by $v_{\mathbf{k}}$) as

$$v_{\mathbf{k}} = i H(z) \frac{d\mathcal{D}_\delta}{dz} \frac{\delta_{\mathbf{k}}}{k}. \quad (\text{A4})$$

H stands for the Hubble function and z for redshift.

The power spectrum for *any* component of the Fourier velocity mode hence reads

$$P_{vv}(k) = \left(H(z) \frac{d\mathcal{D}_\delta(z)}{dz} \right)^2 \frac{P_m(k)}{k^2}. \quad (\text{A5})$$

If we now combine $\delta_{\mathbf{k}}$ and $v_{\mathbf{q}}$, we obtain

$$\langle \delta_{\mathbf{k}} v_{\mathbf{q}}^* \rangle = (2\pi)^3 \delta^D(\mathbf{k} - \mathbf{q}) P_{dv}(k) = (2\pi)^3 \delta^D(\mathbf{k} - \mathbf{q}) i H(z) \frac{d\mathcal{D}_\delta(z)}{dz} \frac{P_m(k)}{k}. \quad (\text{A6})$$

Note that this is an imaginary quantity. In this work, we shall find this power spectrum either squared or in a convolution with itself, giving rise to negative power and indicating *anticorrelation*.

Finally, we compute the power spectrum of the quantity

$$\phi(\mathbf{x}, \mathbf{n}_1) \equiv \delta(\mathbf{x}) (\mathbf{v}(\mathbf{x}) \cdot \mathbf{n}_1) = \sum_i \delta(\mathbf{x}) \left(v_i(\mathbf{x}) n_i^1 \right), \quad (\text{A7})$$

where \mathbf{n}_1 stands for the unitary vector connecting an observer with the position \mathbf{x} , and the sum is over the three spatial components. Since a product in real space involves a convolution in Fourier space, the Fourier mode of ϕ reads:

$$\phi_{\mathbf{k}, \mathbf{n}_1} = \sum_i \int \frac{d\mathbf{q}}{(2\pi)^3} \delta_{\mathbf{q}} v_{i, \mathbf{k} - \mathbf{q}}^1 n_i^1. \quad (\text{A8})$$

Having this in mind, the average product of two Fourier modes of ϕ when looking in two different directions \mathbf{n}_1 and \mathbf{n}_2 is:

$$\langle \phi_{\mathbf{k}, \mathbf{n}_1} \phi_{\mathbf{q}, \mathbf{n}_2}^* \rangle = (2\pi)^3 \delta^D(\mathbf{k} - \mathbf{q}) \left[\cos \theta_{12} [P_{\delta\delta} \star P_{vv}](k) + (\cos \theta_{12} + \sin \theta_{12}) [P_{\delta v} \star P_{v\delta}](k) \right] + (2\pi)^3 \delta^D(\mathbf{k})(2\pi)^3 \delta^D(\mathbf{q}) \left(\int \frac{d\mathbf{u}}{(2\pi)^3} P_{\delta v}(u) \right)^2. \quad (\text{A9})$$

$\theta_{12} = \arccos(\mathbf{n}_1 \cdot \mathbf{n}_2)$ is the angle separating \mathbf{n}_1 and \mathbf{n}_2 . Without introducing any loss of generality of eq.(A9), we have taken $\mathbf{n}_1 = (0, 0, 1)$ and $\mathbf{n}_2 = (0, \sin \theta_{12}, \cos \theta_{12})$. The symbol \star denotes convolution and is present in the first two terms in brackets. The third term is non zero only when $\mathbf{k} = \mathbf{q} = 0$.

Before ending this appendix, it is worth to make some remarks upon the redshift and mass dependence of the power spectra we have computed. The redshift dependence is explicit via the growth factors \mathcal{D}_δ and \mathcal{D}_v . Now, if we are interested in the peculiar velocity of a given cluster, then the (linear) velocity field must be averaged in a sphere of dimensions corresponding to the cluster mass. Something similar can be said about the density field: when studying the dependence of the number of haloes upon the environment density, the field δ must be smoothed on scales which a priori are dependent on the mass of the haloes whose number density we are studying. In this scenario, all Fourier modes of the density and the velocity should be multiplied by the window functions corresponding to the scales within which we are averaging. This introduces a dependence on the masses of the clusters under study in $P_{\delta\delta}$, P_{vv} and $P_{\delta v}$.

APPENDIX B

The Angular correlation function of the projected velocities

Let i and j be two components of the Fourier mode of the peculiar velocity field, so that

$$\left\langle v_{\mathbf{k}}^i (v_{\mathbf{q}}^j)^* \right\rangle = (2\pi)^3 \delta^D(\mathbf{k} - \mathbf{q}) \delta_{ij}^K P_{vv}(k). \quad (\text{B1})$$

Using this, we can write the average product of projected velocities as:

$$\left\langle \left(\mathbf{v}(\mathbf{x}_1) \cdot \mathbf{n}_1 \right) \left(\mathbf{v}(\mathbf{x}_2) \cdot \mathbf{n}_2 \right) \right\rangle =$$

$$\int \frac{k^2 dk}{(2\pi)^3} P_{vv}(k) \left(W(kR_1) W^*(kR_2) \right) \int d\phi d(\cos\theta) \cos\theta_{12} \times \exp -i k [x_1 \cos\theta - x_2 (\sin\theta \cos\phi \sin\theta_{12} + \cos\theta_{12} \cos\theta)]. \quad (\text{B2})$$

In this equation, the polar axis for the \mathbf{k} integration has been taken along the direction given by \mathbf{n}_1 . θ, ϕ are the polar and azimuthal angles of \mathbf{k} , and θ_{12} is the angle separating the two directions of observations, \mathbf{n}_1 and \mathbf{n}_2 . If we now make use of the Rayleigh expansion of the plane wave, i.e.,

$$\exp -i \mathbf{k} \cdot \mathbf{x} = \sum_l (-i)^l (2l+1) j_l(kx) P_l(\mu), \quad (\text{B3})$$

(where μ is the cosine of the angle between \mathbf{k} and \mathbf{x} and P_l are Legendre polynomials), and also the theorem of addition of Legendre functions (see, e.g., Gradshteyn & Ryzhik 8.794), then one ends up with

$$\left\langle \left(\mathbf{v}(\mathbf{x}_1) \cdot \mathbf{n}_1 \right) \left(\mathbf{v}(\mathbf{x}_2) \cdot \mathbf{n}_2 \right) \right\rangle = \sum_{\text{even } l} \frac{2l+1}{4\pi} \cos\theta_{12} \left(\frac{2}{\pi} \mathcal{F}_l \right) \int k^2 dk P_{vv}(k) W(kR_1) W(kR_2) j_l(k[x_1 - x_2 \cos\theta_{12}]) j_l(kx_2 \sin\theta_{12}), \quad (\text{B4})$$

where the factor \mathcal{F}_l is given by

$$\mathcal{F}_l \equiv \frac{(l-1)!!}{2^{l/2} (l/2)!} \cos l \frac{\pi}{2}, \quad (\text{B5})$$

$j_l(x)$ are the spherical Bessel functions and the summation must take place only over *even* values of l . Note that in the limit of $\theta_{12} \rightarrow 0$ and $x_1 \rightarrow x_2$, this expression becomes eq. (2).

At the same time, we can rewrite eq.(B2) as an expansion on Legendre polynomials. Indeed, if we denote by \mathbf{x}_1 and \mathbf{x}_2 the position vectors of the clusters, we can use the Rayleigh expansion of the plane wave for $\exp(i\mathbf{k} \cdot \mathbf{x}_1)$ and $\exp(-i\mathbf{k} \cdot \mathbf{x}_2)$, and write

$$\left\langle \left(\mathbf{v}(\mathbf{x}_1) \cdot \mathbf{n}_1 \right) \left(\mathbf{v}(\mathbf{x}_2) \cdot \mathbf{n}_2 \right) \right\rangle = \sum_{l,l'} (2l+1)(2l'+1)(-i)^{l-l'} \int \frac{d\mathbf{k}}{(2\pi)^3} P_{vv}(k) \cos\theta_{12} j_l(kx_1) j_{l'}(kx_2) P_l(\mu_{\mathbf{k},\mathbf{x}_1}) P_{l'}(\mu_{\mathbf{k},\mathbf{x}_2}), \quad (\text{B6})$$

with $\mu_{\mathbf{x},\mathbf{y}}$ the cosine of the angle formed by vectors \mathbf{x} and \mathbf{y} . Note also that $\mu_{\mathbf{x}_1,\mathbf{x}_2} = \mu_{\mathbf{n}_1,\mathbf{n}_2} = \cos\theta_{12}$. Next we apply the addition theorem of Legendre functions on a spherical triangle formed by $\mathbf{n}_1, \mathbf{n}_2$ and $\hat{\mathbf{k}}$. As before, we take the polar axis of \mathbf{k} to be aligned with \mathbf{x}_1 :

$$\left\langle \left(\mathbf{v}(\mathbf{x}_1) \cdot \mathbf{n}_1 \right) \left(\mathbf{v}(\mathbf{x}_2) \cdot \mathbf{n}_2 \right) \right\rangle = \sum_{l,l'} (2l+1)(2l'+1)(-i)^{l-l'} \int \frac{d\mathbf{k}}{(2\pi)^3} P_{vv}(k) \cos\theta_{12} j_l(kx_1) j_{l'}(kx_2) P_l(\mu_{\mathbf{k},\mathbf{x}_1}) \left[P_{l'}(\mu_{\mathbf{k},\mathbf{x}_1}) P_{l'}(\mu_{\mathbf{x}_1,\mathbf{x}_2}) + \right. \\ \left. 2 \sum_{m=1}^{l'} P_{l'}^m(\mu_{\mathbf{k},\mathbf{x}_1}) P_{l'}^m(\mu_{\mathbf{x}_1,\mathbf{x}_2}) \cos(m[\phi_1 - \phi_2]) \right]. \quad (\text{B7})$$

Because $d\mathbf{k} = k^2 dk \sin\theta d\theta d\phi$, the integration in the azimuthal angle cancels the sum over m in the brackets. Finally, the product $\mu_{\mathbf{x}_1,\mathbf{x}_2} P_l(\mu_{\mathbf{x}_1,\mathbf{x}_2})$ can be rewritten, via a Legendre recurrence relation, as a linear combination of $P_{l-1}(\mu_{\mathbf{x}_1,\mathbf{x}_2})$ and $P_{l+1}(\mu_{\mathbf{x}_1,\mathbf{x}_2})$. After putting all this together, we find

$$\left\langle \left(\mathbf{v}(\mathbf{x}_1) \cdot \mathbf{n}_1 \right) \left(\mathbf{v}(\mathbf{x}_2) \cdot \mathbf{n}_2 \right) \right\rangle = \sum_l \frac{2l+1}{4\pi} C_l^{vv} P_l(\cos\theta_{12}) \quad (\text{B8})$$

where the power spectrum multipoles C_l^{vv} are given by

$$C_l^{vv} = \frac{4\pi}{2l+1} (l\mathcal{B}_{l-1} + (l+1)\mathcal{B}_{l+1}) \quad (\text{B9})$$

and the \mathcal{B}_l 's are defined as

$$\mathcal{B}_l \equiv 4\pi \int \frac{k^2 dk}{(2\pi)^3} P_{vv}(k) j_l(kx_1) j_l(kx_2) \quad (\text{B10})$$

APPENDIX C

The all sky kSZ correlation function

Using eq.(18), we can write the average product of kSZ temperature anisotropies along two directions $\mathbf{n}_1, \mathbf{n}_2$ as

$$\begin{aligned} \left\langle \frac{\delta T_{kSZ}}{T_0}(\mathbf{n}_1) \frac{\delta T_{kSZ}}{T_0}(\mathbf{n}_2) \right\rangle &= \int dr_1 dr_2 dM_1 dM_2 d\mathbf{y}_1 d\mathbf{y}_2 \dot{\tau}(M_1) \dot{\tau}(M_2) W^{gas}(\mathbf{y}_1 - \mathbf{r}_1) W^{gas}(\mathbf{y}_2 - \mathbf{r}_2) \times \\ &\quad \left\langle n(M_1, \mathbf{y}_1) \left(\frac{\mathbf{v}(\mathbf{y}_1)}{c} \cdot \mathbf{n}_1 \right) n(M_1, \mathbf{y}_2) \left(\frac{\mathbf{v}(\mathbf{y}_2)}{c} \cdot \mathbf{n}_2 \right) \right\rangle \end{aligned} \quad (C1)$$

Now we recall our model for the number of haloes of eq.(16) to rewrite the ensemble average in eq.(C1) as

$$\begin{aligned} \left\langle n(M_1, \mathbf{y}_1) \left(\frac{\mathbf{v}(\mathbf{y}_1)}{c} \cdot \mathbf{n}_1 \right) n(M_1, \mathbf{y}_2) \left(\frac{\mathbf{v}(\mathbf{y}_2)}{c} \cdot \mathbf{n}_2 \right) \right\rangle &= \bar{n}(M_1, z_1) \delta^D(M_1 - M_2) \delta^D(\mathbf{y}_1 - \mathbf{y}_2) \sigma_{vv}^2(M_1) + \\ \bar{n}(M_1, z_1) \bar{n}(M_2, z_2) \left\langle \left(\frac{\mathbf{v}(\mathbf{y}_1)}{c} \cdot \mathbf{n}_1 \right) \left(\frac{\mathbf{v}(\mathbf{y}_2)}{c} \cdot \mathbf{n}_2 \right) \right\rangle &+ \frac{\partial \bar{n}(M_1, z_1)}{\partial \delta} \bigg|_{\delta=0} \frac{\partial \bar{n}(M_2, z_2)}{\partial \delta} \bigg|_{\delta=0} \frac{\langle \phi(\mathbf{y}_1, \mathbf{n}_1) \phi(\mathbf{y}_2, \mathbf{n}_2) \rangle}{c^2} \end{aligned} \quad (C2)$$

The first term is the Poisson term, and is zero unless both \mathbf{n}_1 and \mathbf{n}_2 are looking at the same cluster. The second term is the velocity-velocity (vv) term, and the third contains the coupling of density and velocity studied in Appendix A. Plugging eq.(C2) into eq.(C1) and writing the integrands in terms of integrals in Fourier domain, one finds

$$\begin{aligned} \left\langle \frac{\delta T_{kSZ}}{T_0}(\mathbf{n}_1) \frac{\delta T_{kSZ}}{T_0}(\mathbf{n}_2) \right\rangle &= \int dr_1 dr_2 dM_1 d\mathbf{y}_1 \frac{d\mathbf{k}}{(2\pi)^3} \frac{d\mathbf{q}}{(2\pi)^3} e^{-i\mathbf{k}(\mathbf{r}_1 - \mathbf{y}_1) + i\mathbf{q}(\mathbf{r}_2 - \mathbf{y}_1)} W_k^{gas} (W_q^{gas})^* \dot{\tau}^2(M_1) \bar{n}(M_1, z_1) \frac{\sigma_{vv}^2(M_1)}{c^2} + \\ &\int dr_1 dr_2 dM_1 dM_2 \frac{d\mathbf{k}}{(2\pi)^3} \frac{d\mathbf{q}}{(2\pi)^3} e^{-i\mathbf{k} \cdot \mathbf{r}_1 + i\mathbf{q} \cdot \mathbf{r}_2} \bar{n}(M_1, z_1) \bar{n}(M_2, z_2) W_k^{gas} (W_q^{gas})^* \dot{\tau}(M_1) \dot{\tau}(M_2) \left\langle \frac{\mathbf{v}_{\mathbf{k}} \cdot \mathbf{n}_1}{c} \frac{\mathbf{v}_{\mathbf{q}}^* \cdot \mathbf{n}_2}{c} \right\rangle + \\ &\int dr_1 dr_2 dM_1 dM_2 \frac{d\mathbf{k}}{(2\pi)^3} \frac{d\mathbf{q}}{(2\pi)^3} e^{-i\mathbf{k} \cdot \mathbf{r}_1 + i\mathbf{q} \cdot \mathbf{r}_2} \frac{\partial \bar{n}(M_1, z_1)}{\partial \delta} \bigg|_{\delta=0} \frac{\partial \bar{n}(M_2, z_2)}{\partial \delta} \bigg|_{\delta=0} W_k^{gas} (W_q^{gas})^* \dot{\tau}(M_1) \dot{\tau}(M_2) \left\langle \frac{\phi_{\mathbf{k}, \mathbf{n}_1} \phi_{\mathbf{q}, \mathbf{n}_2}^*}{c^2} \right\rangle. \end{aligned} \quad (C3)$$

The integration on \mathbf{y}_1 in the Poisson term generates a Dirac delta on $\mathbf{k} - \mathbf{q}$, whereas in the other two terms this Dirac delta arises naturally when one computes the ensemble average product of the Fourier modes of v and ϕ . Hence, the integral on \mathbf{q} disappears and every integral ends up with a term of the form $\exp i\mathbf{k} \cdot (\mathbf{r}_1 - \mathbf{r}_2)$. We introduce now the Rayleigh expansion, yielding

$$\exp i\mathbf{k} \cdot (\mathbf{r}_1 - \mathbf{r}_2) = \sum_{l, l'} (2l+1)(2l'+1)(-i)^{l-l'} j_l(kr_1) j_{l'}(kr_2) P_l(\mu_{\mathbf{k}, \mathbf{r}_1}) P_{l'}(\mu_{\mathbf{k}, \mathbf{r}_2}), \quad (C4)$$

and we make use (as in eq.(B7) in Appendix B) of the addition theorem of Legendre polynomials to express those Legendre polynomials having as argument $\mu_{\mathbf{k}, \mathbf{r}_2}$ as a sum of Legendre functions of $\mu_{\mathbf{k}, \mathbf{r}_1}$ and $\mu_{\mathbf{r}_1, \mathbf{r}_2}$. Here, as before, we have aligned the polar axis of $\hat{\mathbf{k}}$ along \mathbf{r}_1 or \mathbf{n}_1 . Also in this case, the integral of the azimuthal angle of $\hat{\mathbf{k}}$ cancels the contribution of all Legendre functions having $m \neq 0$, so at the end one is left with

$$\begin{aligned} \left\langle \frac{\delta T_{kSZ}}{T_0}(\mathbf{n}_1) \frac{\delta T_{kSZ}}{T_0}(\mathbf{n}_2) \right\rangle &= \sum_l \frac{2l+1}{4\pi} P_l(\cos \theta_{12}) \left[\int \frac{(4\pi)^2 k^2 dk}{(2\pi)^3} dr_1 dr_2 dM_1 W_k^{gas} (W_q^{gas})^* \dot{\tau}^2(M_1) \frac{\sigma_{vv}^2(M_1)}{c^2} j_l(kr_1) j_l(kr_2) + \right. \\ &\int \frac{(4\pi)^2 k^2 dk}{(2\pi)^3} dr_1 dr_2 dM_1 dM_2 \bar{n}(M_1, z_1) \bar{n}(M_2, z_2) W_k^{gas} (W_q^{gas})^* \dot{\tau}(M_1) \dot{\tau}(M_2) \frac{P_{vv}(k)}{c^2} j_l(kr_1) j_l(kr_2) \cos \theta_{12} + \\ &\int \frac{(4\pi)^2 k^2 dk}{(2\pi)^3} dr_1 dr_2 dM_1 dM_2 \frac{\partial \bar{n}(M_1, z_1)}{\partial \delta} \bigg|_{\delta=0} \frac{\partial \bar{n}(M_2, z_2)}{\partial \delta} \bigg|_{\delta=0} W_k^{gas} (W_q^{gas})^* \dot{\tau}(M_1) \dot{\tau}(M_2) [P_{dd} \star P_{vv}](k) j_l(kr_1) j_l(kr_2) \cos \theta_{12} + \\ &\left. \int \frac{(4\pi)^2 k^2 dk}{(2\pi)^3} dr_1 dr_2 dM_1 dM_2 \frac{\partial \bar{n}(M_1, z_1)}{\partial \delta} \bigg|_{\delta=0} \frac{\partial \bar{n}(M_2, z_2)}{\partial \delta} \bigg|_{\delta=0} W_k^{gas} (W_q^{gas})^* \dot{\tau}(M_1) \dot{\tau}(M_2) [P_{dv} \star P_{vd}](k) j_l(kr_1) j_l(kr_2) \left(\sin \theta_{12} + \cos \theta_{12} \right) \right] \end{aligned} \quad (C5)$$

As in Appendix A, we have taken $\mathbf{n}_1 = (0, 0, 1)$ and $\mathbf{n}_2 = (0, \sin \theta_{12}, \cos \theta_{12})$. Since different velocity components are not correlated, and we are only sensitive to the radial projection of the velocity, a $\cos \theta_{12}$ dependence appears in the vv term. For exactly the same reasons we obtained a $\cos \theta_{12}$ and a $\cos \theta_{12} + \sin \theta_{12}$ dependence when computing the power spectrum of ϕ in Appendix A. Note that, out of the three terms we found in that computation, we have dropped the last one because it is constant and introduces no anisotropy. Since the power spectra multipoles (C_l 's) are projections on Legendre polynomials, such projection must be applied on $\cos \theta_{12}$ and $\cos \theta_{12} + \sin \theta_{12}$. The projection matrix for $\cos \theta_{12}$ will be identical to that given by eq.(B9) in Appendix B. For $\cos \theta_{12} + \sin \theta_{12}$, it must be computed numerically.

Summarising, the power spectra corresponding to each of the terms considered here can be understood as a transformation of some vectors c_l^X (where X runs for *Poisson*, vv , $dd-vv$, $dv-vd$) by some linear applications $\mathcal{A}_{l,l'}^X$:

$$c_l^X = \sum_{l'} \mathcal{A}_{l,l'}^X c_{l'}^X. \quad (C6)$$

For the Poisson term, $\mathcal{A}_{l,l'}^{Poisson}$ is the identity, whereas for the vv and the $dd-vv$ terms we find

$$\mathcal{A}_{l,l'}^{vv, dd-vv} = 4\pi \left[\frac{l \delta_{l-1,l'}^K}{(2l-1)^2} + \frac{(l+1) \delta_{l+1,l'}^K}{(2l+3)^2} \right], \quad (C7)$$

with $\delta_{i,j}^K$ is the Kronecker delta for i and j . The projection matrix for the $dv-vd$ term reads

$$\mathcal{A}_{l,l'}^{dv-vd} = 2\pi \int_{-1}^{+1} d\mu (\mu + \sqrt{1-\mu^2}) P_l(\mu) P_{l'}(\mu). \quad (C8)$$

The c_l^X vectors for the Poisson, vv , $dd-vv$, and $dv-vd$ terms are as follows:

- *Poisson*:

$$c_l^{Poisson} = \frac{2}{\pi} \int k^2 dk dM (\Delta_l^P(k, M))^2, \quad (C9)$$

with $\Delta_l^P(k, M)$ being

$$\Delta_l^P(k, M) = \int dr \dot{\tau} \sigma_{vv} [n(M, z)]^{1/2} j_l(kr) W_k^{gas}. \quad (C10)$$

- vv term:

$$c_l^{vv} = \frac{2}{\pi} \int k^2 dk (\Delta_l^{vv}(k))^2, \quad (C11)$$

with $(\Delta_l^{vv}(k))^2$ given by

$$\left(\Delta_l^{vv}(k) \right)^2 = \int dr_1 dr_2 dM_1 dM_2 \dot{\tau}(M_1, z_1) \dot{\tau}(M_2, z_2) n(M_1, z_1) n(M_2, z_2) W_k^{gas}(M_1, z_1) W_k^{gas}(M_2, z_2) P_{vv}(M_1, M_2, z_1, z_2, k) j_l(kr_1) j_l(kr_2). \quad (C12)$$

- $dd-vv$ term:

$$c_l^{dd-vv} = \frac{2}{\pi} \int k^2 dk (\Delta_l^{dd-vv})^2 \quad (C13)$$

with

$$\left(\Delta_l^{dd-vv}(k) \right)^2 = \int dr_1 dr_2 dM_1 dM_2 \dot{\tau}(M_1, z_1) \dot{\tau}(M_2, z_2) \left. \frac{\partial \bar{n}(M_1, z_1)}{\partial \delta} \right|_{\delta=0} \left. \frac{\partial \bar{n}(M_2, z_2)}{\partial \delta} \right|_{\delta=0} W_k^{gas}(M_1, z_1) W_k^{gas}(M_2, z_2) \times [P_{dd} \star P_{vv}](M_1, M_2, z_1, z_2, k) j_l(kr_1) j_l(kr_2). \quad (C14)$$

- $dv-vd$ term:

$$c_l^{dv-vd} = \frac{2}{\pi} \int k^2 dk (\Delta_l^{dv-vd})^2; \quad (C15)$$

with

$$\left(\Delta_l^{dv-vd}(k) \right)^2 = \int dr_1 dr_2 dM_1 dM_2 \dot{\tau}(M_1, z_1) \dot{\tau}(M_2, z_2) \left. \frac{\partial \bar{n}(M_1, z_1)}{\partial \delta} \right|_{\delta=0} \left. \frac{\partial \bar{n}(M_2, z_2)}{\partial \delta} \right|_{\delta=0} W_k^{gas}(M_1, z_1) W_k^{gas}(M_2, z_2) \times [P_{dv} \star P_{vd}](M_1, M_2, z_1, z_2, k) j_l(kr_1) j_l(kr_2). \quad (C16)$$

REFERENCES

- | | |
|---|---|
| <p>Aghanim, N., Hansen, S. H., & Lagache, G. 2004, ArXiv Astrophysics e-prints, arXiv:astro-ph/0402571</p> <p>Aghanim, N., Górski, K. M., & Puget, J.-L. 2001, A&A, 374, 1</p> <p>Benson B. A., et al., 2003, ApJ, 592, 674</p> <p>Colberg, J. M., et al. 2000, MNRAS, 319, 209</p> | <p>Courteau S., Dekel A., 2001, ASPC, 245, 584</p> <p>DeDeo, S., Spergel, D.N. & Trac, H., 2005, ApJ, <i>submitted</i>, astro-ph/0511060.</p> <p>Diaferio, A., Sunyaev, R. A., & Nusser, A. 2000, ApJL, 533, L71</p> <p>Diaferio, A., et al. 2005, MNRAS, 356, 1477</p> |
|---|---|

- Diego, J. M., Mohr, J., Silk, J., & Bryan, G. 2003, MNRAS, 341, 599
- Doré O., Hennawi J. F., Spergel D. N., 2004, ApJ, 606, 46
- Eisenstein, D.J. et al., 2005, ApJ, *submitted*, astro-ph/0511171
- Fowler et al., 2005, astro-ph/0403137
- Furlanetto S., Loeb A., 2002, ApJ, 579, 1
- Gradshteyn, I.S. & Ryzhik, I.M., 1965, *Table of Integrals, Series and Products*, Academic Press, Inc.
- Gunn, J. E., & Gott, J. R. I. 1972, ApJ, 176, 1
- Hamana, T., Kayo, I., Yoshida, N., Suto, Y., & Jing, Y. P. 2003, MNRAS, 343, 1312
- Holder G. P., 2002, ApJ, 578, L1
- Holder G. P., 2004, ApJ, 602, 18
- Kashlinsky, A. & Atrio-Barandela, F., 2000, ApJ, 536, L67
- Kim, R. S. J., et al. 2002, AJ, 123, 20
- Komatsu, E., & Seljak, U. 2001, MNRAS, 327, 1353
- Komatsu, E., Seljak U., 2002, MNRAS, 336, 1256
- Kosowsky A., 2003, New Astron.Rev. 47, 939
- Linder, E.V., 2005, astro-ph/0507263
- Ma C.-P., Fry J. N., 2002, PhRvL, 88, 211301
- Miller, C.J. et al., 2005, AJ, (*accepted*), astro-ph/0503713
- Mo, H. J., & White, S. D. M. 1996, MNRAS, 282, 347
- Nagai D., Kravtsov A. V., Kosowsky A., 2003, ApJ, 587, 524
- Peebles, P.J.E., 1980, Large Scale Structure of the Universe, Princeton Univ. Press
- Peel, A.C., 2005, astro-ph/0501098
- Ruhl, J., et al. 2004, SPIE, 5498, 11
- Santos, M. G., Cooray, A., Haiman, Z., Knox, L., & Ma, C.-P. 2003, ApJ, 598, 756
- Schäfer, B.M., Pfrommer, C., Bartelmann, M., Springel, V. & Hernquist, L., 2004, MNRAS, *submitted*, (astro-ph/0407089).
- Sehgal, N., Kosowsky, A. & Holder, G., 2005, ApJ, in press, (astro-ph/0504274)
- Sheth, R. K., & Tormen, G. 1999, MNRAS, 308, 119
- Sheth, R. K., & Diaferio, A. 2001, MNRAS, 322, 901
- Spergel D. N., et al. 2003, ApJS, 148, 175
- Strauss, M. A., & Willick, J. A. 1995, PhR, 261, 271
- Sunyaev, R. A., & Zeldovich, Y. B. 1972, Comments on Astrophysics and Space Physics, 4, 173
- Sunyaev, R. A. & Zel'dovich, I. B. 1980, ARA&A, 18, 537
- Tegmark, M. et al., 2004, Phys. Rev.D69, 103501
- Verde, L., Haiman, Z., & Spergel, D. N. 2002, ApJ, 581, 5